Refining the domain architecture model of the replication origin firing factor Treslin/TICRR

Refining the domain architecture model of the replication origin firing factor Treslin/TICRR

Pedro Ferreira[1^*], Luis Sanchez-Pulido[2^], Anika Marko[1], Chris P Ponting[2], Dominik Boos[1*]

[1] Vertebrate DNA Replication Lab, Centre for Medical Biotechnology, University of Duisburg-Essen, 45141 Essen, Germany

[2] Medical Research Council Human Genetics Unit, IGC, University of Edinburgh, Edinburgh EH4 2XU, Scotland, UK

[^] equal contribution

[*] corresponding author: dominik.boos@uni-due.de; phone: +49 201 183 4132, ORCID: https://orcid.org/0000-0003-0018-4375

Running title: Domain architecture of Treslin/TICRR

Key words: DNA Replication, Ku70/Ku80, Metazoa, MTBP/Sld7, Replication Origin Firing, Treslin/TICRR/Sld3

Summary blurb:

The replication origin firing factor Treslin/TICRR comprises an essential Sld3-like core that requires the flanking Ku70-like N-terminal and the C-terminal domains for efficient origin firing.

Abstract

Faithful genome duplication requires appropriately controlled replication origin firing. The metazoan origin firing regulation hub Treslin/TICRR and its yeast orthologue Sld3 share the Sld3-Treslin domain (STD) and the adjacent TopBP1/Dpb11 interaction domain (TDIN). We report a revised domain architecture model of Treslin/TICRR. Protein sequence analyses uncovered a conserved Ku70-homologous β-barrel fold in the Treslin/TICRR middle domain (M domain) and in Sld3. Thus, the Sld3-homologous Treslin/TICRR core comprises its three central domains, M domain, STD and TDIN, flanked by non-conserved terminal domains, the CIT (conserved in Treslins) and the C-terminus. The CIT includes a vWA domain. Unexpectedly, MTBP, Treslin/TICRR and Ku70/80 share the same N-terminal domain architecture, vWA and Ku70-like β-barrels, suggesting a common ancestry. Binding experiments using mutants and the Sld3-Sld7 dimer structure suggest that the Treslin/Sld3 and MTBP/Sld7 β-barrels engage in homotypic interactions, reminiscent of Ku70-Ku80 dimerization. Cells expressing Treslin/TICRR domain mutants indicate that all Sld3-core domains and the non-conserved terminal domains fulfil important functions during origin firing in human cells. Thus, metazoa-specific and widely conserved molecular processes cooperate during metazoan origin firing.

Introduction

Accurate and complete DNA replication guarantees faithful genetic inheritance. It requires complex regulation of replication origin firing to ensure 1) efficient firing to avoid non-replicated gaps, and 2) appropriately controlled firing in space and time to facilitate the metazoan genome replication program and coordinate replication with other chromatin processes like transcription (Berezney et al 2000, Boos & Ferreira 2019, Dileep et al 2015, Helmrich et al 2013, Petryk et al 2016, Ryba et al 2010).

Replication initiation is a two-step process in eukaryotes. The first step, origin licensing, in G1 phase is the formation of pre-replicative complex (pre-RC), the loading of the Mcm2-7 replicative helicase onto double-stranded DNA (Evrin et al 2009, Remus et al 2009). In pre-RCs, the Mcm2-7 complex does not have helicase activity to avoid premature DNA unwinding in G1. The second step is origin firing, the conversion of pre-RCs into two bidirectional replisomes. Firing occurs S phase-specifically due to its dependency on S phase cyclin-dependent kinases (S-CDK) and Dbf4-dependent kinase (DDK), whose activities increase at the G1-S transition. During firing, pre-RCs are first remodelled into pre-initiation complexes (pre-ICs) (Miyazawa-Onami et al 2017, Yeeles et al 2015, Zou & Stillman 1998) that then mature into the active Cdc45-Mcm2-7-GINS-DNA polymerase epsilon (CMGE) helicase (Abid Ali et al 2017, Douglas et al 2018, Ilves et al 2010, Langston et al 2014). DNA synthesis requires assembly of additional replisome factors and primer synthesis (Yeeles et al 2017).

The main regulation step of origin firing is pre-IC formation. In yeast, a dimer of Sld3 and Sld7 (orthologues of metazoan Treslin/TICRR and MTBP (Boos et al 2011, Boos et al 2013,

Kohler et al 2019, Kumagai & Dunphy 2017, Kumagai et al 2010; 2011, Sanchez-Pulido et al 2010, Sansam et al 2010), binds pre-RCs dependently on pre-RC phosphorylation by DDK (Deegan et al 2016, Heller et al 2011). Sld3 recruits Cdc45 via its central STD domain (Itou et al 2014, Kamimura et al 2001) (Fig 1). Sld3 utilizes its TDIN region to bind to Dpb11 (TopBP1/Cut5/Mus101 in higher eukaryotes) in an interaction that depends on phosphorylation at two CDK sites in the TDIN (Boos et al 2011, Zegerman & Diffley 2007). Dpb11 also binds CDK-phosphorylated Sld2 (RecQL4 in higher eukaryotes). Dpb11 and Sld2 form the pre-loading complex together with GINS and DNA polymerase epsilon (Muramatsu et al 2010). The resulting intermediate structure is called pre-IC. Then, Sld3, Dpb11 and Sld2 dissociate and the CMGE helicase forms.

In addition to cell cycle kinases, the DNA damage checkpoint also controls origin firing at the pre-IC step. Checkpoint kinase phosphorylation of Sld3 and Dbf4 inhibits pre-IC formation to avoid mutations through replicating damaged templates (Duch et al 2011, Lopez-Mosqueda et al 2010, Zegerman & Diffley 2010). Recently, it has become clear that more subtle regulation of pre-IC factor activity and levels is critical for faithful genome duplication in yeast (Mantiero et al 2011, Reusswig et al 2016, Tanaka & Araki 2011, Tanaka et al 2011).

Many fundamental processes of yeast origin firing are conserved in vertebrates. All yeast origin firing factors have orthologues in higher eukaryotes (Kohler et al 2019). In addition, cell cycle regulation by CDK through Treslin/Sld3 binding to TopBP1/Dpb11 and also firing inhibition upon DNA damage through suppression of the Treslin/Sld3-TopBP1/Dpb11 interaction are both conserved (Boos et al 2011, Guo et al 2015, Kumagai et al 2010; 2011, Mu et al 2017, Sansam et al 2010).

However, several protein domains of TopBP1, MTBP, Treslin/TICRR and RecQL4 do not have counterparts in yeasts (Kohler et al 2019, Makiniemi et al 2001, Sanchez-Pulido et al 2010, Zegerman 2015). This suggests that, despite the described conservation, metazoa and fungi have evolved specific origin firing processes. Whilst it has been shown that some higher eukaryote-specific domains of MTBP and TopBP1 are required for efficient DNA synthesis (Kohler et al 2019, Kumagai et al 2010), the situation for Treslin/TICRR remains less clear. Characterisation of the protein domains that are specific to higher eukaryotes is essential for defining how origin firing processes in these cells diverge from the established yeast model.

The two central STD and TDIN domains of Treslin/TICRR show sequence-based evidence for homology with Sld3 (Fig 1) (Boos et al 2011, Itou et al 2014, Sanchez-Pulido et al 2010). The molecular functions of the STD of Treslin/TICRR and whether this region is essential for replication remain unknown. Its homology with Sld3 suggests that it might support origin firing through interaction with Cdc45 (Itou et al 2014). The TDIN of Treslin/TICRR is a conserved region containing two CDK phosphorylation sites for TopBP1 binding (Boos et al 2011, Kumagai et al 2011). Like the Sld3-TDIN the Treslin/TICRR-TDIN forms a direct binding surface for BRCA1 C-terminal repeat domains (BRCT) in TopBP1/Dpb11 (Boos et al 2011, Kumagai et al 2011, Zegerman & Diffley 2007).

The Treslin/TICRR domains N- and C-terminal of STD and TDIN (Fig 1) have not been shown to be conserved with Sld3. The M domain shares the ability to bind to MTBP/Sld7 with the N-terminal region of Sld3, and it is required for replication in human cells (Itou et al 2015, Kohler et al 2019). It came as a surprise that sequence conservation with Sld3 was not

detected for the Treslin/TICRR M domain, because the interacting regions in MTBP and Sld7, respectively, show homology via remote but statistically significant sequence similarity (Kohler et al 2019). The region C-terminal of the TDIN is present in many metazoans, but is absent from yeast and plants (Sanchez-Pulido et al 2010). Sequence analysis predicts that this Treslin/TICRR C-terminal region is largely unstructured, with well-conserved stretches of amino acids and more divergent regions alternating. This region binds Chk1 and BRD2/4 (Fig 1), but these activities are not essential for DNA synthesis in cultured human cells (Guo et al 2015, Sansam et al 2018). The N-terminal CIT is conserved in both metazoans and plants, but not present in fungi (Sanchez-Pulido et al 2010). Whether the CIT functions in replication is unknown.

We here define the essential Sld3-like core of Treslin/TICRR as the three M, STD and TDIN domains, flanked by higher eukaryote-specific terminal domains. Moreover, we characterise structurally and functionally the M domain and the higher eukaryote-specific terminal regions.

Results

The M domain, the STD and the TDIN domain constitute the essential core of Treslin/TICRR

We first sought to better define the essential core domains of Treslin/TICRR for replication. Mutations of Treslin/TICRR previously showed that the MTBP/Sld7-binding M domain and the TopBP1/Dpb11-binding TDIN perform essential functions during origin firing in human cells (Boos et al 2011, Boos et al 2013, Kumagai & Dunphy 2017). In contrast, the requirement of the Sld3-homologous STD for replication had not previously been addressed in higher eukaryotes. To test this, we used incorporation of the nucleotide analogue 5-

bromo-2'-deoxyuridine (BrdU) into nascent DNA of cultured human cells in an established RNAi-replacement system (Boos et al 2011, Boos et al 2013). U2OS cell clones stably expressing siRNA-resistant Treslin/TICRR wild type (WT) or STD-deletion mutants (ΔSTD, amino acids 717-792 deleted) to similar levels were treated with control siRNA (siCtr) or Treslin/TICRR siRNA (siTreslin) (Fig 2A; Fig S1A (Blots with siRNA); Fig S2A-E (data processing strategy)). Cells were pulse-labelled with BrdU 72 h after transfection, stained with anti-BrdU-FITC and propidium iodide (PI), and analysed by flow cytometry. Parental U2OS cells and control cell lines expressing the inactive non-TopBP1 interacting CDK site mutant Treslin/TICRR-2PM showed severely reduced BrdU incorporation levels compared to siCtr-treated cells (Fig 2B). Whilst Treslin/TICRR-WT rescued BrdU incorporation, three independent clones expressing Treslin/TICRR-ΔSTD (clones 11, 17 and 21) showed strong defects in supporting replication (Fig 2B). Quantification of the average replication-dependent BrdU signal in replicates (Fig 2C) (Boos et al 2013, Ferreira et al 2021, Kohler et al 2019) confirmed these observations. Treslin/TICRR-ΔSTD clone 21 rescued replication somewhat better (50 % replication) than clones 11 (approximately 30 % replication; 2PM and no-transgene controls about 30%), exemplifying our observation that individual clones expressing the same transgene showed some variability that probably arise through clonal selection, prompting us to 1) always use more than one clone per mutant throughout the project, and 2) not over-interpret subtle differences between mutants that show less clear defects than Treslin/TICRR-ΔSTD. We then tested if specifically the origin firing step of replication is impaired in Treslin/TICRR-ΔSTD cells by analysing origin licensing and replisome formation on chromatin. Western blotting of chromatin fractions using anti-Mcm2 antibodies showed that replication origin licensing occurred normally in the G1 phase (4 h after Nocodazole release) in Treslin/TICRR-ΔSTD cells. In contrast, origin firing did not

occur in the absence of the STD domain as indicated by severely reduced S phase-specific (12 h) Cdc45 and PCNA loading onto chromatin (Fig 2D). The loss of replication activity is not a consequence of a delay in S phase entry, because Cyclin A accumulated normally in Treslin-ΔSTD cells 12 h after release (Fig 2D), and because Treslin/TICRR-ΔSTD cells have a high proportion of S phase cells (Fig 2Bii, PI profiles). We sought to confirm the conclusion that Treslin-ΔSTD cells replicate slowly due to a defect in origin firing. In an attempt to exclude secondary effects that may complicate interpretation of the presented flow cytometry end point assays (Fig 2B,C), the cells were treated such that the analysed S phase was the first after replacing endogenous Treslin/TICRR with siRNA-resistant transgenes. For this, we monitored cells released from a double thymidine block. A significant fraction of Treslin-WT cells doubled their DNA content within 10 h after release from thymidine, whereas Treslin/TICRR-ΔSTD and Treslin/TICRR-2PM cells accumulated DNA much slower (Fig S3A and B). The fact that any significant DNA synthesis occurred in Treslin/TICRR-ΔSTD, Treslin/TICRR-2PM and U2OS control cells is likely due to the suboptimal siRNA treatment conditions required in this synchronisation regime (short treatment, only one siRNA round). Immunoblotting chromatin fractions for pre-RC formation (licensing) and replisome formation (firing) revealed that all cell lines contained high levels of pre-RCs in the thymidine arrest (0 h) (Fig S3C and D). In Treslin/TICRR-WT cells, pre-RCs became largely cleared from chromatin 10 h after release, consistent with Mcm proteins being eliminated from chromatin during genome replication through replication termination and passive replication of origins. In contrast, Treslin/TICRR-ΔSTD, Treslin/TICRR-2PM and U2OS control cells retained high Mcm2 protein levels 10 h after release, consistent with replication of a large portion of their genome remaining incomplete. Replisomes (PCNA on chromatin) were visible in Treslin/TICRR-WT control cells at early time points, but were severely decreased

after 10 h, consistent with genome replication being nearly complete 10 h after release. Lower levels of replisomes also formed in Treslin/TICRR-ΔSTD and Treslin/TICRR-2PM and U2OS control cells due to the inefficient siRNA treatment. However, replisomes were not cleared from the chromatin throughout the entire time course, consistent with slow replication (Fig S3C and D). STD deletion neither led to gross misfolding of Treslin/TICRR nor affected the described activities of the neighbouring M and TDIN domains, because Treslin-ΔSTD immunoprecipitated MTBP (Boos et al 2013) and TopBP1 (Fig S4A and B) normally. Treslin-ΔSTD localised to the nucleus normally (Fig S5). We concluded from these RNAi-rescue experiments that deleting the STD severely compromises replication origin firing in U2OS cells. Thus, the STD is part of the essential set of core domains of Treslin/TICRR, together with the M and TDIN domains.

Characterisation of the region N-terminal to the Treslin/TICRR-STD by protein sequence analysis

We then sought to better understand the region N-terminal to the STD of Treslin/TICRR. This has no described sequence conservation with Sld3, but contains the M domain that has a conserved activity – the binding to MTBP/Sld7 – and is part of the essential Treslin/TICRR core. To do so we inspected the Treslin/TICRR structure, predicted by AlphaFold a recently developed machine learning approach that yields high accuracy (Tunyasuvunakool et al., 2021; Jumper et al., 2021). This predicted structure contained an N-terminal von Willebrand factor type A (vWA) fold (also known as a Rossmann fold, corresponding to the CIT), a β-barrel (corresponding to the M domain, residues 299 to 424) and the α-helical STD domain (Fig S6A). Unexpectedly, the β-barrel domain was structurally similar to the yeast Ku70 structure (PDB:5y58_A, residues 264 to 451; Chen et al., 2018) with a Dali Z-score of 13.3

and a root-mean-square deviation (RMSD) of 2.6Å (Fig S7). Additional similarities were noted to the known structures of Sld7 (PDB:3x37_B, residues 3 to 119; Z-score = 8.6; RMSD = 3.1Å) and Sld3 (PDB:3x37_A, residues 4 to 75; Z-score = 3.1; RMSD = 2.9Å), thereby identifying Ku70-like β-barrels in both the Sld3 binding domain of yeast Sld7 and the Sld7-binding domain of Sld3 (PDB-ID: 3X37_B) (PDB-ID: 3X37_A) (Figs 3A and S8A-C) (Itou et al 2015). The Sld3 β-barrel is truncated, containing only five β-strands (Fig S8A). It is notable that the Sld3/Sld7 heterodimer forms in a structurally equivalent manner to the Ku70/Ku80 heterodimer, specifically a homotypic dimer of two structurally similar domains.

Structural similarity could be the result of divergent evolution (i.e. homology) or convergent evolution (i.e. analogy). To distinguish these possibilities, we used iterative profile-to-sequence (HMMer) and profile-to-profile comparisons (HHpred) (Eddy 1996, Finn et al 2011, Soding et al 2005). HHpred searches against the PDB70 profile database (Soding et al 2005), used the previously identified CIT region that is conserved between animal and plant Treslins (corresponding to residues 4 to 254 of human Treslin/TICRR) (Sanchez-Pulido et al 2010) (Fig 1). This search identified the Treslin/TICRR von vWA domain as homologous to the vWA domain of human complement factor B protein (PDB-ID: 3HRZ_D) (Janssen et al 2009) (*E*-value = 9.2×10^{-3}; true positive probability of 97%) (Fig S7). The secondary structure prediction for this region of Treslin/TICRR showed good agreement with the known secondary structure known of diverse members of the vWA superfamily (Jones 1999) (Fig S7).

In a similar manner, HHpred searches of the Treslin/TICRR M domain against the PDB70 profile database (Soding et al 2005) yielded statistically significant sequence similarity to

yeast Ku70 (PDB-ID: 5Y58_E) (Chen et al 2018) (*E*-value = 0.3; true positive probability of 88%) (Fig 3A). In further support of homology, the next most statistically significant matches were to three further members of the Ku family, namely yeast Ku80 (PDB-ID: 5Y58_F) (Chen et al 2018), human XRCC5 (PDB-ID: 1JEY_B), and human XRCC6 (X-ray repair cross-complementing protein 6) (PDB-ID: 1JEY_A) (Walker et al 2001). Both sequence conservation (HHpred) and Alphafold structure prediction thus provided strong and consistent evidence that the conserved M domain in Treslin/TICRR adopts a Ku70-like β-barrel containing seven core β-strands (Fig. 3A and S8). Additionally, the structural similarities of the β-barrel domains for Sld3 and Sld7 and their respective human orthologues Treslin/TICRR and MTBP suggest that the Ku70-like β-barrel newly identified in Treslin/TICRR (M domain) is an excellent candidate for being the principal region (heterodimerization domain) that interacts with MTBP.

The Ku70-like β-barrel of Treslin/TICRR is required for interaction with MTBP

We next tested whether Treslin/TICRR and MTBP may indeed interact via a homotypic Ku70/Ku80-type β-barrel-dependent interaction. Previous biochemical and structural studies had shown that MTBP/Sld7 regions, now established here as part of their β-barrels, interact with Treslin/Sld3 (Itou et al 2015, Kohler et al 2019).

We showed previously that deleting two large regions of the Treslin/TICRR M domain, amino acids 265-408 (M1) or 409-593 (M2), compromised MTBP binding (Boos et al 2013). Deleting M2 abrogated and deleting M1 severely weakened this interaction. Figure 3B shows that a fragment of Treslin/TICRR containing amino acids 260-671 that included M1 and M2 co-immunoprecipitated with endogenous MTBP in lysates of transfected 293T cells.

To test the involvement of the Ku70-like β-barrel in Treslin/TICRR, we deleted amino acids 370-400 and 401-420, each containing portions that aligned with Sld3 regions that make direct contacts with Sld7 (Fig 3A, * symbols) (Itou et al 2015). Both deletions severely compromised the interaction with MTBP (Fig 3B), indicating that the β-barrel is required. To confirm and specify the results from these large deletions we mutated the three β-strands in the 370-420 region individually (Fig S9A). All strands contain amino acids whose Sld3-equivalents contact Sld7 (Fig 3A, * symbols) (Itou et al 2015). Seeking to change the amino acid sequence yet preserve the overall structure, we replaced the β-strands by unrelated β-strand forming sequences. Fig S9B shows that all mutations weakened but did not abrogate binding to MTBP. These results are consistent with β-strands in the Treslin/TICRR β-barrel contributing to the MTBP interaction surface that correspond to Sld3/Sld7-interacting strands yet cannot rule out more indirect effects of these mutations.

We found that a region C-terminal to the Ku70-like β-barrel is also required for MTBP interaction. The N-terminal 557 amino acids of Treslin/TICRR, but not the N-terminal 486 amino acids, bound to MTBP (Fig 3B). Small deletions revealed that the amino acids 518-543, but not 487-517 and 545-557, are required for MTBP binding (Fig 3B). This region contains a small loop and an α-helical part C-terminal of the β -barrel fold (Fig S6A). In yeast Sld3, a short sequence approximately 35 amino acids C-terminal to the β-barrel also contains six amino acids that directly contact Sld7 (Itou et al 2015). We conclude that the Ku70-like β-barrel in the Treslin/TICRR M domain cooperates with a second region further to the C-terminus in binding to MTBP. We cannot exclude an indirect contribution of the amino acid 518-543 region to dimerization, although its position in an apparently independent folding unit from the β-barrel makes it unlikely that its deletion destabilised the β-barrel.

Together, our analysis of the N-terminal 600 amino acids of Treslin/TICRR revealed that the structurally conserved part with Sld3 includes the Ku70/80-like β-barrel in the M domain. Thus, the central part of the Treslin/TICRR protein including the M, STD and TDIN domains constitutes a core that is homologous to Sld3, flanked by Treslin/TICRR-specific terminal domains. Moreover, Treslin/TICRR, MTBP and Ku70/Ku80 share an N-terminal domain structure comprising a vWA domain followed by Ku70-like β-barrel domains (Fig S6A, B).

The Sld3-homologous Treslin/TICRR core is insufficient to support replication

We next wanted to test whether the Sld3-like Treslin/TICRR core is sufficient to support replication in human cells or whether it requires the higher eukaryote-specific CIT and C-terminal domains. We performed BrdU-PI flow cytometry upon RNAi-replacement of Treslin/TICRR using mutants that lacked either the CIT (Treslin/TICRR-ΔCIT, amino acids 1-264 deleted), the C-terminal region (Treslin/TICRR-ΔC853, C-terminal 853 amino acids deleted), or both (Treslin/TICRR-core) (Fig 4A). Treslin/TICRR-ΔCIT and Treslin/TICRR-ΔC853 cells showed relatively normal BrdU-PI profiles compared to Treslin/TICRR-WT cells, with S phase populations clearly separated from G1 and G2/M cells by higher BrdU signal intensities (Fig 4B). Quantification of multiple independent experiments indicated only minor reductions in Treslin/TICRR-ΔCIT and Treslin/TICRR-ΔC853 lines (Fig 4C). Testing additional clones confirmed these results (Fig S10A, B, D and E), although, as described for Treslin/TICRR-ΔSTD, there was some clone-to-clone variability, with one of three ΔC853 clones (no. 29) rescuing like Treslin/TICRR-WT (Fig S10E). Expression levels of Treslin/TICRR-ΔC853 clones were similar or higher than Treslin/TICRR-WT (Fig S10B and D, and S1B). The observed clone-to-clone variability makes a clear assessment difficult whether

306 Treslin/TICRR-ΔCIT and ΔC853 are mildly compromised or support DNA replication like
307 Treslin-WT.
308
309 Surprisingly, the Treslin/TICRR-core mutant was inactive. BrdU incorporation in
310 Treslin/TICRR-core cells was nearly as strongly compromised as in the non-replicating
311 control lines (Fig 4B and C, additional clones in Fig S11A-C). This indicated that, albeit
312 individually non-essential for replication, simultaneous deletion of both terminal regions
313 had an additive or even synergistic effect on DNA replication. Treslin/TICRR-core localised
314 normally to the nucleus (Fig S5). Together, the strong reproducible replication defect
315 observed with Treslin/TICRR-core mutants warrants the conclusion that the Sld3-like core
316 domains of Treslin/TICRR require the CIT domain and the C-terminal region to support
317 replication in human cells.
318
319 *The CIT cooperates with amino acids 1057-1257 in the C-terminus to support origin firing.*
320 We then tested which part of the C-terminal region cooperates with the CIT, and whether
321 the cooperation depends on the described binding activities for Chk1 and BRD2/4. We
322 successively truncated the C-terminal sequence in combination with CIT deletion. Neither
323 truncating the Chk1- (Treslin/TICRR-ΔCIT/ΔC99) (Guo et al 2015) nor the Chk1- and BRD2/4-
324 binding domains (Treslin/TICRR-ΔCIT/ΔC651) (Sansam et al 2018) recapitulated the
325 synergistic effect (Fig 4A-C; additional clones in Figs S11B,D,E and S12A,B,C,E). These
326 double-deletion mutants supported replication to a similar level as Treslin/TICRR-ΔCIT and
327 WT. The C-terminal truncations Treslin/TICRR-ΔC651 and ΔC99 (that contained the CIT) did
328 not greatly affect BrdU incorporation (Figs S10C and S12B). We confirmed these results with

two independent double-deletion mutants: Treslin/TICRR-ΔCIT/ΔC309 that contains the BRD2/4 binding site, and Treslin/TICRR-ΔCIT/ΔC394 that does not (Fig S12A, D and E).

Treslin/TICRR-core did not support replication, as described above. To test whether the known core activities of Treslin/TICRR are intact in the Treslin/TICRR-core protein we tested association with MTBP and TopBP1. Treslin/TICRR-core and ΔC853 co-immunoprecipitated TopBP1 from 293T cell lysates similarly as Treslin/TICRR-ΔC651 (with or without CIT), suggesting that C-terminal deletion of the important amino acids 1057-1257 did not detectably compromise TopBP1 binding (Fig S13A, lanes 4-7 and B, lanes 4 and 6). Comparison of Treslin/TICRR-core and ΔC853 with Treslin/TICRR-full-length was difficult because of differences in expression levels and blotting efficiency in transient transfections as a result of considerable size differences. Treslin/TICRR-core also bound MTBP. Some experiments (that had the same limitations as explained for TopBP1 binding experiments) suggested slightly less MTBP bound to Treslin/TICRR-core than to Treslin/TICRR-WT (Figs 4D and S13A,B), which could indicate that the vWA domain-containing CIT makes a small contribution to MTBP binding, similarly to the vWA domain in Ku70/Ku80 (Walker et al 2001). We cannot formally rule out that potential mild reductions in binding capability of Treslin/TICRR-core to MTBP and TopBP1 fully explains the strong replication deficiency of Treslin/TICRR-core, although this is less likely.

We therefore suggest that two higher eukaryote-specific Treslin/TICRR regions (specifically, CIT and the C-terminal amino acids 1057-1257) have important functions in replication.

Treslin/TICRR-core expressing cells are defective in origin firing

Subtle particularities in cell cycle profiles of Treslin/TICRR-core cells suggested that this mutant may have other defects than cells lacking Treslin/TICRR function. For example, a delay in S phase entry in Treslin/TICRR-core cells could explain the occasionally observed decrease of the S phase sub-population (Fig S11C, clone 41). To exclude such secondary effects of long-term siRNA treatment as much as possible, we next analysed the first S phase after replacing endogenous with transgenic Treslin/TICRR. We tested whether Treslin/TICRR-core cells licensed origins normally and progressed normally into S phase, but showed a defect in origin firing in. To this end, we released Treslin/TICRR-core-expressing cells and U2OS control cells from a thymidine arrest into a nocodazole block and treated them with siRNA such that they completed S phase before siTreslin could take effect. Upon nocodazole wash-out, U2OS cells typically start replicating at around 7 h, so we chose 4 h and for 12 h to analyse BrdU-PI profiles and replisome formation. All cell lines exited from the nocodazole arrest and entered G1 phase, as indicated by 2 C DNA content at the 4 h time point (Fig 5A). As usual, a subpopulation of cells released from the arrest with a delay. Subpopulations of siCtr-treated U2OS cells and siTreslin-treated Treslin/TICRR-WT cells had started BrdU incorporation 12 h after nocodazole release. The fastest of these replicating cells had duplicated a significant portion of their genome, as judged by PI signals, showing that they had been replicating for several hours. In contrast, siTreslin-treated Treslin/TICRR-core and control cells incorporated BrdU at nearly undetectable levels. We confirmed that Treslin/TICRR-core cells have a severe defect in genome replication using cells released from a double thymidine arrest. Upon release from the arrest, Treslin/TICRR-core cells accumulated DNA much slower that Treslin/TICRR-WT cells, as measured by propidium iodide staining (Fig S3A and B). In addition, immunoblotting of chromatin fractions with Mcm2 and PCNA antibodies revealed that Treslin/TICRR-core cells did not clear pre-RCs

from chromatin and replisomes were still visible 10 h after thymidine release (Fig S3E and F). We then tested whether Treslin/TICRR-core expressing cells have defects specifically at the origin firing step of DNA replication, but complete origin licensing and G1-S progression normally. For this, we analysed whole cell lysates and chromatin isolated from nocodazole-released cells. The Mcm2-7 helicase loaded normally onto chromatin in siTreslin-treated Treslin/TICRR-core G1 cells (4 h), showing that licensing was intact (Fig 5B). A cyclin A band was detectable in whole cell lysates after 12 h but not after 4 h in all cell lines, suggesting that Treslin/TICRR core progressed normally into S phase (Fig 5C). In contrast, replisomes did not form more efficiently with Treslin/TICRR-core than in cells without transgenic Treslin/TICRR, as indicated by PCNA and Cdc45 signals on chromatin at 12 h in Treslin/TICRR-WT cells, but not in Treslin/TICRR-core and control cells (Fig 5B). The very low signals of Cdc45 and PCNA at 12 h may stem from the siRNA not suppressing endogenous Treslin/TICRR to 100%. We conclude that Treslin/TICRR-core is specifically defective in origin firing.

Together, the Treslin/TICRR terminal regions that are specific to higher eukaryotes cooperate in parallel pathways towards an essential function in replication origin firing.

Discussion

We here present a characterization of a major origin-firing regulator, Treslin/TICRR, based on its domain structure. Our insight that Treslin/TICRR and Sld3 share similarity of the M domain (Treslin/TICRR) and the N-terminus (Sld3), respectively, completes the view that the three central domains of Treslin/TICRR, M-domain, STD and TDIN, constitute a Sld3-like core that is flanked by two Treslin/TICRR-specific terminal regions, the CIT and the C-terminal

region (Fig 6). These terminal regions are required for Treslin/TICRR's role in replication origin firing.

Important molecular activities of the core domains are known. TDIN is essential for replication in Sld3 and Treslin/TICRR through CDK-mediated interaction with Dpb11 and TopBP1, respectively (Boos et al 2011, Kumagai et al 2011, Tanaka et al 2007, Zegerman & Diffley 2007). The Sld3-STD binds Cdc45 (Itou et al 2014), an essential component of the replicative CMG helicase. Although the Cdc45-binding activity of the STD has not been investigated in Treslin/TICRR, conservation with Sld3 suggests that this biochemical activity might also be conserved (Itou et al 2014). Consistently, we show here that the Treslin/TICRR-STD is required for replication origin firing in cultured human cells, confirming that it has retained important replication functions in humans. The M domain of Treslin/TICRR is also essential for replication in human cells and mediates the binding to MTBP (Boos et al 2013). Itou et al. showed that the M domain-equivalent of Sld3 constitutes a direct binding surface for Sld7 (Itou et al 2015). We reported earlier that the M domain interacting region in MTBP, approximately the N-terminal MTBP half, contains homology to the Sld3-binding N-terminus of Sld7 (Kohler et al 2019). Here we show that the interaction is mediated by Ku70-like β-barrel domains in Treslin/TICRR/Sld3 and MTBP/Sld7 (Itou et al 2015, Kohler et al 2019), suggesting that they form homotypic dimers comprised of structurally similar domains, similar to Ku70-Ku80 dimerization (Walker et al 2001). Uncharacterised important molecular activities might be situated in the regions between the Treslin/TICRR domains with proven homology to Sld3, such as the DDK-dependent binding to the Mcm2-7 helicase shown for a short stretch of amino acids between the STD and TDIN of Sld3 (Deegan et al 2016).

We found that the Sld3-like core of Treslin/TICRR was insufficient to support replication and origin firing in U2OS cells, whereas individual deletions of the Treslin/TICRR-specific CIT and C-terminus had only mild effects, if any (given the uncertainty due to clonal variability), on Treslin/TICRR's ability to support replication. We concluded that the CIT and the C-terminal region cooperate in parallel pathways to promote DNA replication origin firing. The simplest scenario is that CIT and the C-terminal region promote firing through functions in the molecular process of origin firing that have yet to be revealed. However, more indirect scenarios cannot be excluded. Our finding supports the idea of molecular processes and regulations that are specific to higher eukaryotes to facilitate faithful duplication of their extremely complex genomes. Previous publications had shown roles for higher eukaryote-specific protein domains of TopBP1 (Kumagai et al 2010) and MTBP (Kohler et al 2019).

The molecular activities underlying the proposed origin firing functions of CIT and the C-terminal region remain unknown. Our mutants combining CIT-deletion and successive C-terminal truncation excluded significant contributions of the described Chk1- and BRD2/4-binding regions of the Treslin/TICRR C-terminus (Guo et al 2015, Sansam et al 2018). Instead, comparing the Treslin-ΔCIT/Δ853 with Treslin-ΔCIT/Δ651 mutants suggested that the relevant activity is situated between amino acids 1057 and 1257 of human Treslin/TICRR. Because this region is very close to the TDIN we considered that TopBP1 binding could be compromised in Treslin-Δ853. Although minor defects of Treslin/TICRR-Δ853 mutants in TopBP1 binding cannot be formally excluded we found no clear evidence for a TopBP1 binding deficiency, regardless of whether or not the CIT was present. Also the fact that Treslin-Δ853 mutants that contain the CIT have mild or no defects in supporting genome replication, depending on the clone observed, argues against a significant TopBP1

449 binding deficiency. A relevant activity in the CIT for origin firing may be to support the
450 binding to MTBP for two reasons: 1) Treslin/TICRR-core and Treslin/TICRR-ΔCIT bound
451 somewhat less well to MTBP (Fig 4D and (Kohler et al 2019)), and 2) the CIT-equivalent
452 domain in Ku70/80 makes a small contribution to the Ku70/80 dimer interface (Walker et al
453 2001). This potential mild MTBP binding defect may contribute to the inability of
454 Treslin/TICRR-core to support origin firing. However, we find it unlikely that such a
455 moderate defect fully explains the strong replication deficiency of Treslin/TICRR-core. This
456 view is supported by the fact that a Sld3/Sld7-type interaction does not necessarily require a
457 CIT, because Sld3-Sld7 dimerization is CIT-independent. We cannot formally exclude that
458 Treslin/TICRR-core is prone to unfolding, although its normal expression levels, good
459 TopBP1 and MTBP binding capability and normal nuclear localisation speak against this.
460 Other labs also reported that C-terminally deleted Treslin/TICRR-ΔC651 supported
461 replication well (Kumagai et al 2010), suggesting that C-terminal truncation is compatible
462 with Treslin/TICRR's capability to support replication.
463
464 Interestingly, the CIT contains a vWA domain that is also shared by 1) Ku70/Ku80 (Walker et
465 al 2001) and 2) by MTBP (Fig 6). A specific molecular activity cannot be delineated from the
466 presence of a vWA domain since these domains in other proteins have a variety of activities.
467 The Ku70/80 similarities supports speculation that, during evolution, Treslin/TICRR and
468 MTBP received the vWA and β-barrel domains in a single event of genomic recombination.
469 The identical order of the domains in the Ku70/80 proteins suggests that Ku proteins,
470 Treslin/TICRR, and MTBP share an ancestral donor for these domains or that one of the
471 three was the ancestor. Because animal and plant Treslins (but not yeast) contain CITs, the
472 last common ancestor of plants and animals likely contained a CIT. As opisthokonts, fungi

and animals are more closely related to each other than animals are to plants, so the CIT must have been lost from Sld3 during yeast evolution. In conclusion, the CIT may have been "donated" to Treslin/TICRR as one unit alongside the Ku70-like β-barrel. Both together had the capability to form homotypic dimers with MTBP. The minor (or absent) contribution of the CIT to MTBP binding presents the possibility that it was retained in most branches of evolution due to another function important for eukaryotic cells.

Determining the molecular and cellular functions of the non-core Treslin/TICRR domains will help us better understand the specifics of origin firing in higher eukaryotes compared to yeast. Because Treslin/TICRR mediates origin firing regulation, understanding its non-core domains will likely be necessary to unravel how the complex higher eukaryotic cells coordinate origin firing with other cellular processes.

Materials and Methods

Cell culture

U2OS (ATCC-HTB-96) and 293T (ATCC CRL-11268) cells (both lines kind gift from The Crick institute tissue culture) were cultured in standard conditions in DMEM/high glucose (Life Technologies, 41965062), 10 % FCS, Penicillin/Streptomycin in 5 % CO_2. Stable AcGFP-Flag-GFP-Treslin/TICRR-expressing U2OS cell clones were generated using a pIRES puro3-based vector system by random genome integration followed by selection on 0.3 µg/ml puromycin and picking of individual clones as described (Boos et al 2011, Boos et al 2013).

Analysis of unsynchronised and synchronous stable U2OS cells by BrdU-flow cytometry and chromatin analysis

Endogenous Treslin/TICRR was replaced by siTreslin-resistant transgenes by transfecting U2OS cells twice with Treslin/TICRR siRNA (GAACAAAGGTTATCACAAA) using RNAiMax (Life Techmologies/ 13778150) as described (Boos et al 2011). Luciferase siRNA (GL2, Dharmacon) served as a control. For end point analysis of unsynchronised cells, cells were labelled with 10 µM BrdU for 30 min 72 h after the first transfection, harvested and stained with anti-BrdU-FITC (Becton Dickinson/ 556028) and propidium iodide as described (Boos et al 2011). Flow cytometry analysis was performed, analyzed and quantified as described (Kohler et al 2019). In brief, for quantification of replication rescue using BrdU-PI flow cytometry, the BrdU signal intensity of the S phase cell population was background-subtracted using the combined BrdU-channel signal of G1 and G2/M populations to determine the replication-dependent BrdU signal, as shown in Fig S2A-E. This replication signal was normalized to the replication signal of siCtr-treated cells of the same cell clone to calculate the relative replication rescue. For analysis of synchronized U2OS cells in Fig 2D

and E cells were arrested by treatments with 2 mM thymidine for 18 h, release for 10 h, and arrested once again with 2 mM thymidine for 18 h. 4 h after release from the second thymidine block cells were treated with siRNA and 100 µg/ml nocodazole was added for 16h. Release from the nocodazole arrest was done by washing the cells twice. After cultivation for four or twelve hours, cells were harvested and analysed by BrdU-flow cytometry as described above or by immunoblotting of whole cell lysates or chromatin-enriched fractions as described (Boos et al 2013). For Fig 5, cells were instead treated with siRNA and arrested by treatment with 2 mM thymidine for 20 h. Upon release from the thymidine block, 100 µg/ml nocodazole was added for 18h. Cells were treated with the second round of siRNA 4 h after the start of the nocodazole arrest. For Fig S3 cells were arrested by treatment with 2 mM thymidine for 20h, released for 10h, and arrested a second time with 2 mM thymidine for 18h. Cells were treated with siTreslin or siCtr 8 h after release from the first thymidine arrest. Finally, cells were released from the second thymidine block, harvested 0 h, 6 h or 20 h after release and analysed by PI-flow cytometry or by immunoblotting of chromatin-enriched fractions as described above.

Antibodies and affinity matrices

Antibodies against Treslin, MTBP and TopBP1 were described (Boos et al 2011, Boos et al 2013, Kohler et al 2019). Anti-BrdU-FITC (Becton Dickinson/ 556028); anti-HA (mouse, 16B12; Covance); anti-GFP nanobodies (kind gift from Kirill Alexandrov); anti-GFP (mouse, JL-8, Clonetech, 632381), anti-Mcm2 (goat, sc-9839, Santa Cruz), anti-Mcm5 (rabbit, ab17967, abcam), anti-Cdc45 (rat, 3G10, kind gift from Helmut Pospiech), anti-PCNA (mouse, sc-56, Santa Cruz), NHS sepharose (Fisher Scientific, 10343240), Protein G magnetic beads (Life Technologies, 10004D)

Immunoprecipiation from transiently transfected 293T cell lysates

293T cells were transfected using standard calcium phosphate precipitation. 72 h after transfection, cells were harvested and lysed in 5-10 times cell pellet volume using detergent in native lysis buffers and douncing. Lysis buffer for anti-GFP immunoprecipitations in Fig S11 was 20mM Hepes, 250mM NaCl, 10% Glycerol, 0,1%Triton, 2mM EDTA, 10mM NaF, 2mM mM ß-Mecaptoethanol, Complete EDTA-free protease inhibitors (Roche, 5056489001); for Fig 4D lysis buffer was 20mM Hepes, 300mM NaCl, 10% Glycerol, 0,1%Triton, 2mM EDTA, 2mM mM ß-Mecaptoethanol, Complete EDTA-free protease inhibitors (Roche, 5056489001); for rabbit anti-MTBP immunoprecipitation in Fig 3B 20mM Hepes, 200mM NaCl, 10% Glycerol, 0,1%Triton, 2mM mM ß-Mecaptoethanol, Complete EDTA-free protease inhibitors. Lysates from cells from 12.5 % (Fig 3B) and 100 % (Figs 4D, S3 S11) confluent 10 cm dish (Figs S3 and S11), as well as 10 µl (Figs S3, S11 and 4D) GFP nanobody NHS sepharose beads (1 µg/µl) or 1 µg anti-MTBP (amino acids 1-284) antibody on 10 µl magnetic protein G slurry beads (Fig 3B) were used per reaction. After washing three time with lysis buffer beads were boiled in Laemmli loading buffer and analysed by SDS PAGE and immunoblotting. For CDK treatment of lysates, 67 µg/ml bacterially purified Cdk2-cyclin A (purification system generously donated by Tim Hunt), 5 mM ATP and 5 mM $MgCl_2$ were added to the lysis buffers.

Computational protein sequence analysis

Multiple sequence alignments were generated with the program T-Coffee using default parameters (Notredame et al., 2000), slightly refined manually and visualized with the Belvu program (Sonnhammer and Hollich, 2005). Profiles of the alignment as global hidden

Markov models (HMMs) were generated using HMMer (Eddy, 1996; Finn et al., 2011). Profile-based sequence searches were performed against the Uniref50 protein sequence database (Wu et al., 2006) using HMMsearch (Eddy, 1996; Finn et al., 2011). Profile-to-profile comparisons were performed using HHpred (Söding et al., 2005). Profile-to-sequence (HMMer) and Profile-to-profile (HHpred) matches were evaluated in terms of an E-value, which is the expected number of non-homologous proteins with a score higher than that obtained for the database match. An E-value much lower than one indicates statistical significance. Secondary structure predictions were performed using PsiPred (Jones, 1999). Protein structures and models were analysed using Pymol (http://www.pymol.org). Structure similarity searches and structural superpositions were performed using Dali (Holm, 2020).

Data availability

The authors will comply with Life Science Alliance policies for the sharing of research materials and data.

Acknowledgements

We would like to thank the members of the S Westermann, H Meyer and D Boos labs for discussion and sharing expertise and regents.

Author contributions

Conceptualization: D.B., P.F.; Data Curation: P.F., L.S.P, D.B., C.P.P.; Formal analysis: P.F., L.S.P, D.B.; Funding acquisition: D.B., C.P.P.; Investigation: P.F., L.S.P, A.M., D.B.;

Methodology: P.F., L.S.P, C.P.P., D.B.; Development of methodology: P.F., L.S.P. D.B.; Acquisition of data: P.F., L.S.P, A.M., D.B.; Project administration: D.B.; Supervision: D.B., C.P.P.; Validation: P.F., L.S.P, A.M., C.P.P., D.B.; Visualization: P.F., L.S.P, D.B.; Analysis and interpretation of data: P.F., L.S.P, A.M., C.P.P., D.B.; Writing (original draft, review and editing): D.B. P.F., L.S.P

Conflict of interest

The authors declare no conflict interest.

References

Abid Ali F, Douglas ME, Locke J, Pye VE, Nans A, Diffley JFX, Costa A. 2017. Cryo-em structure of a licensed DNA replication origin. Nat Commun. 8(1):2241. doi:10.1038/s41467-017-02389-0

Berezney R, Dubey DD, Huberman JA. 2000. Heterogeneity of eukaryotic replicons, replicon clusters, and replication foci. Chromosoma. 108(8):471-484.

Boos D, Ferreira P. 2019. Origin firing regulations to control genome replication timing. Genes (Basel). 10(3) doi:10.3390/genes10030199

Boos D, Sanchez-Pulido L, Rappas M, Pearl LH, Oliver AW, Ponting CP, Diffley JFX. 2011. Regulation of DNA replication through sld3-dpb11 interaction is conserved from yeast to humans. Curr Biol. 21(13):1152-1157. doi:10.1016/j.cub.2011.05.057

Boos D, Yekezare M, Diffley JF. 2013. Identification of a heteromeric complex that promotes DNA replication origin firing in human cells. Science. 340(6135):981-984. doi:10.1126/science.1237448

Chen H, Xue J, Churikov D, Hass EP, Shi S, Lemon LD, Luciano P, Bertuch AA, Zappulla DC, Geli V, et al. 2018. Structural insights into yeast telomerase recruitment to telomeres. Cell. 172(1-2):331-343 e313. doi:10.1016/j.cell.2017.12.008

Cormier A, Campbell MG, Ito S, Wu S, Lou J, Marks J, Baron JL, Nishimura SL, Cheng Y. 2018. Cryo-em structure of the alphavbeta8 integrin reveals a mechanism for stabilizing integrin extension. Nat Struct Mol Biol. 25(8):698-704. doi:10.1038/s41594-018-0093-x

Deegan TD, Yeeles JT, Diffley JF. 2016. Phosphopeptide binding by sld3 links dbf4-dependent kinase to mcm replicative helicase activation. EMBO J. 35(9):961-973. doi:10.15252/embj.201593552

Dileep V, Ay F, Sima J, Vera DL, Noble WS, Gilbert DM. 2015. Topologically associating domains and their long-range contacts are established during early g1 coincident with the establishment of the replication-timing program. Genome Res. 25(8):1104-1113. doi:10.1101/gr.183699.114

Douglas ME, Ali FA, Costa A, Diffley JFX. 2018. The mechanism of eukaryotic cmg helicase activation. Nature. 555(7695):265-268. doi:10.1038/nature25787

Duch A, Palou G, Jonsson ZO, Palou R, Calvo E, Wohlschlegel J, Quintana DG. 2011. A dbf4 mutant contributes to bypassing the rad53-mediated block of origins of replication in response to genotoxic stress. J Biol Chem. 286(4):2486-2491. doi:10.1074/jbc.M110.190843

Eddy SR. 1996. Hidden markov models. Curr Opin Struct Biol. 6(3):361-365. doi:10.1016/s0959-440x(96)80056-x

Evrin C, Clarke P, Zech J, Lurz R, Sun J, Uhle S, Li H, Stillman B, Speck C. 2009. A double-hexameric mcm2-7 complex is loaded onto origin DNA during licensing of eukaryotic DNA replication. Proc Natl Acad Sci U S A. 106(48):20240-20245. doi:10.1073/pnas.0911500106

Ferreira P, Hofer V, Kronshage N, Marko A, Reusswig KU, Tetik B, Diessel C, Kohler K, Tschernoster N, Altmuller J, et al. 2021. Mtbp phosphorylation controls DNA replication origin firing. Sci Rep. 11(1):4242. doi:10.1038/s41598-021-83287-w

Finn RD, Clements J, Eddy SR. 2011. Hmmer web server: Interactive sequence similarity searching. Nucleic Acids Res. 39(Web Server issue):W29-37. doi:10.1093/nar/gkr367

637 Guo C, Kumagai A, Schlacher K, Shevchenko A, Shevchenko A, Dunphy WG. 2015. Interaction
638 of chk1 with treslin negatively regulates the initiation of chromosomal DNA
639 replication. Mol Cell. 57(3):492-505. doi:10.1016/j.molcel.2014.12.003
640 Heller RC, Kang S, Lam WM, Chen S, Chan CS, Bell SP. 2011. Eukaryotic origin-dependent
641 DNA replication in vitro reveals sequential action of ddk and s-cdk kinases. Cell.
642 146(1):80-91. doi:10.1016/j.cell.2011.06.012
643 Helmrich A, Ballarino M, Nudler E, Tora L. 2013. Transcription-replication encounters,
644 consequences and genomic instability. Nat Struct Mol Biol. 20(4):412-418.
645 doi:10.1038/nsmb.2543
646 Holm L. 2020. Using dali for protein structure comparison. Methods Mol Biol. 2112:29-42.
647 doi:10.1007/978-1-0716-0270-6_3
648 Holm L, Sander C. 1995. Dali: A network tool for protein structure comparison. Trends
649 Biochem Sci. 20(11):478-480. doi:10.1016/s0968-0004(00)89105-7
650 Ilves I, Petojevic T, Pesavento JJ, Botchan MR. 2010. Activation of the mcm2-7 helicase by
651 association with cdc45 and gins proteins. Mol Cell. 37(2):247-258.
652 doi:10.1016/j.molcel.2009.12.030
653 Itou H, Muramatsu S, Shirakihara Y, Araki H. 2014. Crystal structure of the homology domain
654 of the eukaryotic DNA replication proteins sld3/treslin. Structure. 22(9):1341-1347.
655 doi:10.1016/j.str.2014.07.001
656 Itou H, Shirakihara Y, Araki H. 2015. The quaternary structure of the eukaryotic DNA
657 replication proteins sld7 and sld3. Acta Crystallogr D Biol Crystallogr. 71(Pt 8):1649-
658 1656. doi:10.1107/S1399004715010457
659 Janssen BJ, Gomes L, Koning RI, Svergun DI, Koster AJ, Fritzinger DC, Vogel CW, Gros P. 2009.
660 Insights into complement convertase formation based on the structure of the factor
661 b-cobra venom factor complex. EMBO J. 28(16):2469-2478.
662 doi:10.1038/emboj.2009.184
663 Jones DT. 1999. Protein secondary structure prediction based on position-specific scoring
664 matrices. J Mol Biol. 292(2):195-202. doi:10.1006/jmbi.1999.3091
665 Jumper J, Evans R, Pritzel A, Green T, Figurnov M, Ronneberger O, Tunyasuvunakool K, Bates
666 R, Zidek A, Potapenko A, et al. 2021. Highly accurate protein structure prediction
667 with alphafold. Nature. 596(7873):583-589. doi:10.1038/s41586-021-03819-2
668 Kamimura Y, Tak YS, Sugino A, Araki H. 2001. Sld3, which interacts with cdc45 (sld4),
669 functions for chromosomal DNA replication in saccharomyces cerevisiae. Embo J.
670 20(8):2097-2107.
671 Kohler K, Sanchez-Pulido L, Hofer V, Marko A, Ponting CP, Snijders AP, Feederle R, Schepers
672 A, Boos D. 2019. The cdk8/19-cyclin c transcription regulator functions in genome
673 replication through metazoan sld7. PLoS Biol. 17(1):e2006767.
674 doi:10.1371/journal.pbio.2006767
675 Kumagai A, Dunphy WG. 2017. Mtbp, the partner of treslin, contains a novel DNA-binding
676 domain that is essential for proper initiation of DNA replication. Mol Biol Cell.
677 doi:10.1091/mbc.E17-07-0448
678 Kumagai A, Shevchenko A, Dunphy WG. 2010. Treslin collaborates with topbp1 in triggering
679 the initiation of DNA replication. Cell. 140(3):349-359. doi:10.1016/j.cell.2009.12.049
680 Kumagai A, Shevchenko A, Dunphy WG. 2011. Direct regulation of treslin by cyclin-
681 dependent kinase is essential for the onset of DNA replication. J Cell Biol. 193(6):995-
682 1007. doi:10.1083/jcb.201102003

683 Langston LD, Zhang D, Yurieva O, Georgescu RE, Finkelstein J, Yao NY, Indiani C, O'Donnell
684 ME. 2014. Cmg helicase and DNA polymerase epsilon form a functional 15-subunit
685 holoenzyme for eukaryotic leading-strand DNA replication. Proc Natl Acad Sci U S A.
686 111(43):15390-15395. doi:10.1073/pnas.1418334111
687 Lopez-Mosqueda J, Maas NL, Jonsson ZO, Defazio-Eli LG, Wohlschlegel J, Toczyski DP. 2010.
688 Damage-induced phosphorylation of sld3 is important to block late origin firing.
689 Nature. 467(7314):479-483. doi:10.1038/nature09377
690 Makiniemi M, Hillukkala T, Tuusa J, Reini K, Vaara M, Huang D, Pospiech H, Majuri I,
691 Westerling T, Makela TP, et al. 2001. Brct domain-containing protein topbp1
692 functions in DNA replication and damage response. J Biol Chem. 276(32):30399-
693 30406.
694 Mancias JD, Goldberg J. 2007. The transport signal on sec22 for packaging into copii-coated
695 vesicles is a conformational epitope. Mol Cell. 26(3):403-414.
696 doi:10.1016/j.molcel.2007.03.017
697 Mantiero D, Mackenzie A, Donaldson A, Zegerman P. 2011. Limiting replication initiation
698 factors execute the temporal programme of origin firing in budding yeast. EMBO J.
699 30(23):4805-4814. doi:10.1038/emboj.2011.404
700 Miyazawa-Onami M, Araki H, Tanaka S. 2017. Pre-initiation complex assembly functions as a
701 molecular switch that splits the mcm2-7 double hexamer. EMBO Rep. 18(10):1752-
702 1761. doi:10.15252/embr.201744206
703 Mu R, Tat J, Zamudio R, Zhang Y, Yates JR, 3rd, Kumagai A, Dunphy WG, Reed SI. 2017. Cks
704 proteins promote checkpoint recovery by stimulating phosphorylation of treslin. Mol
705 Cell Biol. 37(20) doi:10.1128/MCB.00344-17
706 Muramatsu S, Hirai K, Tak YS, Kamimura Y, Araki H. 2010. Cdk-dependent complex
707 formation between replication proteins dpb11, sld2, pol (epsilon}, and gins in
708 budding yeast. Genes Dev. 24(6):602-612. doi:10.1101/gad.1883410
709 Notredame C, Higgins DG, Heringa J. 2000. T-coffee: A novel method for fast and accurate
710 multiple sequence alignment. J Mol Biol. 302(1):205-217.
711 doi:10.1006/jmbi.2000.4042 S0022-2836(00)94042-7
712 Petryk N, Kahli M, d'Aubenton-Carafa Y, Jaszczyszyn Y, Shen Y, Silvain M, Thermes C, Chen
713 CL, Hyrien O. 2016. Replication landscape of the human genome. Nat Commun.
714 7:10208. doi:10.1038/ncomms10208
715 Ponting CP, Schultz J, Copley RR, Andrade MA, Bork P. 2000. Evolution of domain families.
716 Adv Protein Chem. 54:185-244. doi:10.1016/s0065-3233(00)54007-8
717 Remus D, Beuron F, Tolun G, Griffith JD, Morris EP, Diffley JFX. 2009. Concerted loading of
718 mcm2-7 double hexamers around DNA during DNA replication origin licensing. Cell.
719 139(4):719-730. doi:10.1016/j.cell.2009.10.015
720 Reusswig KU, Zimmermann F, Galanti L, Pfander B. 2016. Robust replication control is
721 generated by temporal gaps between licensing and firing phases and depends on
722 degradation of firing factor sld2. Cell Rep. 17(2):556-569.
723 doi:10.1016/j.celrep.2016.09.013
724 Ryba T, Hiratani I, Lu J, Itoh M, Kulik M, Zhang J, Schulz TC, Robins AJ, Dalton S, Gilbert DM.
725 2010. Evolutionarily conserved replication timing profiles predict long-range
726 chromatin interactions and distinguish closely related cell types. Genome Res.
727 20(6):761-770. doi:10.1101/gr.099655.109
728 Sanchez-Pulido L, Diffley JFX, Ponting CP. 2010. Homology explains the functional similarities
729 of treslin/ticrr and sld3. Curr Biol. 20(12):R509-510. doi:10.1016/j.cub.2010.05.021

730 Sansam CG, Pietrzak K, Majchrzycka B, Kerlin MA, Chen J, Rankin S, Sansam CL. 2018. A
731 mechanism for epigenetic control of DNA replication. Genes Dev. 32(3-4):224-229.
732 doi:10.1101/gad.306464.117
733 Sansam CL, Cruz NM, Danielian PS, Amsterdam A, Lau ML, Hopkins N, Lees JA. 2010. A
734 vertebrate gene, ticrr, is an essential checkpoint and replication regulator. Genes
735 Dev. 24(2):183-194. doi:10.1101/gad.1860310
736 Soding J, Biegert A, Lupas AN. 2005. The hhpred interactive server for protein homology
737 detection and structure prediction. Nucleic Acids Res. 33(Web Server issue):W244-
738 248. doi:10.1093/nar/gki408
739 Sonnhammer EL, Hollich V. 2005. Scoredist: A simple and robust protein sequence distance
740 estimator. BMC Bioinformatics. 6:108. doi:10.1186/1471-2105-6-108
741 Tanaka S, Araki H. 2011. Multiple regulatory mechanisms to inhibit untimely initiation of
742 DNA replication are important for stable genome maintenance. PLoS Genet.
743 7(6):e1002136. doi:10.1371/journal.pgen.1002136
744 Tanaka S, Nakato R, Katou Y, Shirahige K, Araki H. 2011. Origin association of sld3, sld7, and
745 cdc45 proteins is a key step for determination of origin-firing timing. Curr Biol.
746 21(24):2055-2063. doi:10.1016/j.cub.2011.11.038
747 Tanaka S, Umemori T, Hirai K, Muramatsu S, Kamimura Y, Araki H. 2007. Cdk-dependent
748 phosphorylation of sld2 and sld3 initiates DNA replication in budding yeast. Nature.
749 445(7125):328-332. doi:10.1038/nature05465
750 Tunyasuvunakool K, Adler J, Wu Z, Green T, Zielinski M, Zidek A, Bridgland A, Cowie A,
751 Meyer C, Laydon A, et al. 2021. Highly accurate protein structure prediction for the
752 human proteome. Nature. 596(7873):590-596. doi:10.1038/s41586-021-03828-1
753 Vangone A, Spinelli R, Scarano V, Cavallo L, Oliva R. 2011. Cocomaps: A web application to
754 analyze and visualize contacts at the interface of biomolecular complexes.
755 Bioinformatics. 27(20):2915-2916. doi:10.1093/bioinformatics/btr484
756 Walker JR, Corpina RA, Goldberg J. 2001. Structure of the ku heterodimer bound to DNA and
757 its implications for double-strand break repair. Nature. 412(6847):607-614.
758 doi:10.1038/35088000
759 Whittaker CA, Hynes RO. 2002. Distribution and evolution of von willebrand/integrin a
760 domains: Widely dispersed domains with roles in cell adhesion and elsewhere. Mol
761 Biol Cell. 13(10):3369-3387. doi:10.1091/mbc.e02-05-0259
762 Wu CH, Apweiler R, Bairoch A, Natale DA, Barker WC, Boeckmann B, Ferro S, Gasteiger E,
763 Huang H, Lopez R, et al. 2006. The universal protein resource (uniprot): An
764 expanding universe of protein information. Nucleic Acids Res. 34(Database
765 issue):D187-191. doi:10.1093/nar/gkj161
766 YYeeles JT, Deegan TD, Janska A, Early A, Diffley JF. 2015. Regulated eukaryotic DNA
767 replication origin firing with purified proteins. Nature. 519(7544):431-435.
768 doi:10.1038/nature14285
769 Yeeles JT, Janska A, Early A, Diffley JF. 2017. How the eukaryotic replisome achieves rapid
770 and efficient DNA replication. Mol Cell. 65(1):105-116.
771 doi:10.1016/j.molcel.2016.11.017
772 Zegerman P. 2015. Evolutionary conservation of the cdk targets in eukaryotic DNA
773 replication initiation. Chromosoma. 124(3):309-321. doi:10.1007/s00412-014-0500-y
774 Zegerman P, Diffley JFX. 2007. Phosphorylation of sld2 and sld3 by cyclin-dependent kinases
775 promotes DNA replication in budding yeast. Nature. 445(7125):281-285.
776 doi:10.1038/nature05432

777 Zegerman P, Diffley JFX. 2010. Checkpoint-dependent inhibition of DNA replication initiation
778 by sld3 and dbf4 phosphorylation. Nature. 467(7314):474-478.
779 doi:1038/nature09373
780 Zou L, Stillman B. 1998. Formation of a preinitiation complex by s-phase cyclin cdk-
781 dependent loading of cdc45p onto chromatin. Science. 280(5363):593-596.
782

Figure legends

Figure 1 – Treslin/TICRR domain structure

CIT: Conserved in Treslins; M: middle domain; STD: Sld3-Treslin domain; TDIN: TopBP1/Dpb11 interaction domain. Numbers indicate amino acid position in human Treslin/TICRR or budding yeast Sld3. Arrows point to interacting proteins: MTBP binds to the Treslin/TICRR M domain, Cdc45 binds to the STD domain of Sld3 (unknown for Treslin/TICRR), TopBP1 binds to a region containing the two CDK phospho-serine (2xP) residues T969 and S1001 (Boos et al 2011, Kumagai et al 2011), Chk1 binds to the very C-terminal 99 amino acids of Treslin (Guo et al 2015) and Brd2/4 binds to the Treslin/TICRR region 1560-1580 (Sansam et al 2018).

Figure 2 – The STD domain of Treslin/TICRR is required for DNA replication in cultured human cells

(A) Whole cell lysates of stable U2OS cell lines carrying siRNA resistant transgenes of Treslin/TICRR-WT, Treslin/TICRR-2PM (threonine 969 and serine 1001 double alanine mutant that cannot interact with TopBP1(Boos et al 2011)) or three clones of Treslin/TICRR with a deletion of the STD (amino acids 717-792 deleted) were immunoblotted with rabbit anti-Treslin/TICRR (amino acids 1566-1909) antibodies. Ponceau (Ponc.) staining controlled for loading (Load.).

(B) Cells described in A were treated with control or Treslin/TICRR siRNAs (siCtr/siTres) before analysis by flow cytometry detecting BrdU (5-bromo-2'-deoxyuridine; logarithmic (log.) scale) and PI (propidium iodide; linear (lin.) scale). Density plots (i) and PI profiles (ii) are shown. Dashed lines indicating peak level of maximal BrdU incorporation in each cell line

upon siCtr-treatment allow visual comparison with level upon siTres treatment. PI profiles histograms show relative cell count.

(C) Quantification of relative overall DNA replication in cells described in A based on flow cytometry experiments described in B. Averages of BrdU-replication signals of two experiments. Replication signals of siTreslin-treated cells were normalised to replication signals of the same cell line upon siCtr-treatments.

(D) Stable U2OS cell lines expressing siTreslin-resistant Treslin/TICRR-ΔSTD, WT or 2PM were released from a double thymidine arrest before treatment with siTreslin and nocodazole. After nocodazole-release for 4 h or 12 h cells chromatin was isolated for immunoblotting with goat anti-Mcm2, rat anti-Cdc45 and mouse anti-PCNA antibodies. Whole cell lysates from the same samples were immunoblotted using mouse anti-cyclin A and goat anti-Mcm2 antibodies. For each antibody, crops are from the same immunoblot exposure. Coomassie (Coom.) staining of low molecular weight part including histones controlled for loading. Clone Treslin-ΔSTD -11 was used.

Figure 3 – Treslin/TICRR, Sld3 and Sld7 contain a Ku70/80-like β-barrel that are required for Treslin/Sld3-MTBP/Sld7 dimerization

(A) Representative multiple sequence alignment of Ku70-like β-barrel domain in the Treslin/TICRR family. The alignment generated with the program T-Coffee (Notredame et al 2000) using default parameters and slightly refined manually. The final alignment was obtained using a combination of profile-to-profile comparisons (Soding et al 2005) and sequence alignments derived from structural super-positions of a selection of Ku70-like β-barrel domains whose tertiary structure is known (Holm & Sander 1995). The limits of the protein sequences included in the alignment are indicated by flanking residue positions.

Secondary structure prediction using PsiPred (Jones 1999) was performed for the Treslin family, shown in the first lane; this prediction is consistent with the secondary structure of Ku70-like β-barrel domains, shown below each of the proteins with known structure (Ku70, PDB:5Y58E; Ku80, PDB:5Y58F; SPOC, PDB:1OW1A; Sld7, PDB:3X37B; Sld3, PDB:3X37A). Alpha-helices and β-strands are indicated by H and E, respectively. The alignment was presented with the program Belvu using a colouring scheme indicating the average BLOSUM62 scores (which are correlated with amino acid conservation) of each alignment column: black (>3), grey (between 3 and 1.5) and light grey (between 1.5 and 0.5) (Sonnhammer & Hollich 2005). Sequences are named according to their specie common name or abbreviation corresponding as follow to their UniProt identification and specie name (Wu et al 2006):Human, Q7Z2Z1_HUMAN, *Homo sapiens*; Mouse, Q8BQ33_MOUSE, *Mus musculus*; Sarha, G3WMD4_SARHA; *Sarcophilus harrisii*; Chicken, E1BU88_CHICK; *Gallus gallus*; Frog, D3IUT5_XENLA, *Xenopus laevis*; Latch, H3BCK8_LATCH, *Latimeria chalumnae*; Tetng, H3CYF8_TETNG, *Tetraodon nigroviridis*; Collu, A0A4U5UGV6_COLLU, *Collichthys lucidus*; Lepoc, W5ND48_LEPOC, *Lepisosteus oculatus*; 9tele, A0A3B3T1X9_9TELE, *Paramormyrops kingsleyae*; Ictpu, A0A2D0SG01_ICTPU, *Ictalurus punctatus*; Fish, Q6DRL4_DANRE, *Danio rerio.* Blue asterisks: amino acid positions in Sld3 that mediate Sld7 interaction (Itou et al 2015)

(B) Schematic representation of Treslin/TICRR mutants (i) used for interaction studies (ii). For (ii), the indicated N-terminally 3HA-tagged Treslin/TICRR fragments were transiently transfected into 293T cells before immunoprecipitation from cell lysates using control IgG (IgG IP) or rabbit anti-MTBP (amino acids 1-284) (MTBP-IP). Lysates and precipitates were immunoblotted with detection by rat anti-MTBP (12H7) and anti-HA antibodies. VWA: von Willebrand A domain; β, β-barrel

Figure 4 – The CIT and the region between amino acids 1057-1257 of Treslin/TICRR cooperate to support replication in human cells

(A) Schematic representation of Treslin/TICRR mutants used in this figure. Δ: deletion; C99, 651, 853: C-terminal 99, 651 or 853 amino acids, Chk1 kinase binding requires the C-terminal 99 amino acids, BRD2/4 binds to a region between amino acids 1515 and 1600 that were deleted in Treslin/TICRR-ΔC651, -ΔC853, -ΔC394 and -ΔC309 (latter two mutants shown in Fig S5), respectively. ΔCIT, amino acids 1-264 deleted.

(B) Flow cytometry density plots (i) and PI profiles (ii) of experiments as described in Fig 2B using the stable U2OS cell lines expressing siTreslin-resistant Treslin/TICRR mutants described in A. PI profiles histograms show relative cell count. Cell clones: ΔC853-5, ΔCIT(-C-full)-5; ΔCIT-ΔC99-25; ΔCIT-ΔC651-61; core-35.

(C) Quantification of relative overall replication as described in Fig 2C of several independent experiments as described in B). Cell clones as in B; Error bars: SEM; sample numbers (n): 8 (none; WT), 5 (ΔCIT(-C-full); ΔC853), 3 (ΔCIT-ΔC99; ΔCIT-ΔC651; core); significance tests: parametric, unpaired, two tailed student t-test, *P≤0.05.

(D) Immunoblot with mouse anti-GFP or rat anti-MTBP (12H7) antibodies of co-immunoprecipitation experiment using 293T cells transiently transfected with GFP-Flag-Treslin/TICRR-WT or core. Native lysates were immunoprecipitated with anti-GFP nanobodies (GFP-IP) or empty control beads (Ctr. IP).

Figure 5 – Treslin/TICRR-core does not support replisome formation

(A) Stable U2OS cell lines expressing no transgene or siTreslin-resistant Treslin/TICRR-WT or core were released from a thymidine arrest before treatment with siTreslin or siCtr and

879 nocodazole. After nocodazole-release for 4 h or 12 h cells were analysed by BrdU-PI flow
880 cytometry. Clone Treslin/TICRR-core-35 was used.
881 **(B)** Chromatin of cells treated as described in A was isolated for immunoblotting with rabbit
882 anti-Mcm5, rat anti-Cdc45 and mouse anti-PCNA antibodies. Coomassie (Coom.) staining of
883 low molecular weight part including histones controlled for loading. In the high exposure
884 (exp.) the strongest band is saturated.
885 **(C)** Whole cell lysates of cells treated as described in A were immunoblotted using mouse
886 anti-cyclin A antibody.
887
888 **Figure 6 – Common domain architecture of Treslin/TICRR/Sld3, MTBP and Ku70/Ku80**
889 **proteins.**
890 Domain models of the indicated proteins. Abbreviations: vWA, von Willebrand factor type A
891 domain; β: Ku70/80-like β-barrel; STD, Sld3-Treslin domain; 8B, Cdk8/19-cyclin C binding
892 domain; S7M, Sld7/MTBP C-terminal domain; Numbers indicate amino acids position and
893 protein length. In Sld3 and Treslin/TICRR are indicated two conserved CDK phosphorylated
894 S/TP sites (Sld3, position 600 and 622; Treslin/TICRR, position 669, 1001);
895
896
897

Supplementary figure legends

Supplementary figure S1 – RNAi-replacement of endogenous Treslin/TICRR in U2OS-Flip-In cell lines

(A) siRNA against Treslin/TICRR (siTres) specifically eliminates endogenous, but not siRNA-resistant GFP-Flag-Treslin/TICRR transgenes (Boos et al 2011, Boos et al 2013). Whole cell lysates of U2OS cells or U2OS cells expressing RNAi-resistant Treslin/TICRR-wild type (WT) or Treslin/TICRR-ΔSTD-clone11 were treated with no siRNA (-), control siRNA (siCtr) or siRNA against Treslin/TICRR (siTres) as indicated and analysed by immunoblotting using anti-Treslin/TICRR (148) and Ponceau (Pon.) staining. Note that endogenous Treslin/TICRR and GFP-Flag-Treslin/TICRR-WT migrate very similarly on SDS polyacrylamide gels.

(B) Whole cell lysates of U2OS cells expressing RNAi-resistant Treslin/TICRR-wild type (WT), Treslin/TICRR-core-clone35, Treslin/TICRR-ΔCIT-clone5 or Treslin/TICRR-ΔC853-clone5 were treated and analysed as described in A, except that immunoblotting was done using anti-Treslin/TICRR (30E7), since the antibody anti-Treslin/TICRR (148) used in A recognizes a region of Treslin/TICRR not present in the core and ΔC853 mutants. Treslin/TICRR-wild type (WT) samples are the same immunoblotted in A. All samples shown in A and B were processed in parallel. Treslin/TICRR-core runs as a more distinct band than WT due to the absence of the highly posttranslationally modified C-terminus.

Supplementary figure S2 – Gating and data processing strategy for BrdU-PI flow cytometry

(A) Forward and side scatter plot and BrdU-PI profiles of ungated data from a sample of U2OS cells treated with siCtr. The indicated threshold was used in the forward scatter channel to eliminate small debris.

(B) Strategy used for cell doublet (aggregates of 2 cells) discrimination of sample shown in A.

(C) Gates used to discriminate between S-phase (BrdU positive) and Non-S-phase (BrdU negative) cells. Same gates were used within individual experiments. Average BrdU signal intensity was then calculated for each cell population based on the geometric mean of the signal intensities in the BrdU channel.

(D) To calculate BrdU dependent replication signal, the BrdU signal intensity of the S phase cell population was background-subtracted using the signal intensity of the non-S-phase population.

(E) Replication of siTreslin treated cells was normalised to siCtr treated cells to calculate the relative replication rescue.

Supplementary figure S3 – Treslin/TICRR-ΔSTD and Treslin/TICRR-core expressing cells progress slower through S-phase

(A) Stable U2OS cell lines expressing no transgene or siTreslin-resistant GFP-Flag-Treslin/TICRR-WT, 2PM, ΔSTD or core were arrested in a double thymidine block and treated with siTreslin or siCtr 8 h after release from the first thymidine arrest, so that the siRNA would take effect only after the genome had been replicated. After release for 0h, 6h, or 10h from the second thymidine block, cells were analysed by PI flow cytometry. Histograms show overlays between the samples for the three time points and the gates used to calculate amount of cells in early S-phase and late S-phase, respectively. PI histograms show relative cell count. Clones Treslin/TICRR-ΔSTD-11 and Treslin/TICRR-core-35 were used.

(B) Quantification of number of cells in early S-phase or late S-phase, 0h and 10h after a double thymidine release of samples described in A, using the gates show in A. At 0h after

946 release, all samples show around 70 % of cells in early S-phase, consistent with similar
947 synchronization by the double thymidine arrest. 10 h after release, U2OS cells treated with
948 siCtr and Treslin/TICRR-WT expressing cells treated with siTreslin show almost 60 % of cells
949 had progressed to late S-phase, with 10 to 20% remaining in early-S-phase. In contrast, only
950 around 30 % U2OS cells treated with siTreslin and cells expressing Treslin/TICRR-2PM, ΔSTD,
951 or core had progressed to late-S-phase by 10 h. This shows that Treslin/TICRR-ΔSTD or core
952 expressing cells replicated at similar rates as cells expressing the inactive Treslin/TICRR-2PM
953 mutant or cells lacking Treslin/TICRR, indicating that Treslin/TICRR-ΔSTD and core do not
954 support normal S-phase replication.
955 **(C/E)** Chromatin of cells shown in A were isolated for immunoblotting with goat anti-Mcm2
956 and mouse anti-PCNA antibodies. Coomassie (Coom.) staining of low molecular weight part
957 including histones controlled for loading. Samples shown in C and E are the same shown in A
958 and were processed in parallel. 10 h after double thymidine release, U2OS cells treated with
959 siCtr and Treslin/TICRR-WT expressing cells treated with siTreslin show that pre-RCs became
960 largely cleared from chromatin, and replisomes (PCNA on chromatin) were also severely
961 decreased, consistent with genome replication being nearly complete at 10 h. In contrast, in
962 U2OS cells treated with siTreslin and in cells expressing Treslin/TICRR-2PM, ΔSTD, or core,
963 pre-RCs and replisomes were cleared from chromatin at much slower rates, consistent with
964 slow replication.
965 **(D)** Quantification of Mcm2 (i) and PCNA (ii) signals of immunoblots shown in C.
966 **(F)** Quantification of Mcm2 (i) and PCNA (ii) signals of immunoblots shown in E.
967
968 **Supplementary figure S4 – Treslin/TICRR-ΔSTD is proficient in binding TopBP1**

(A) GFP-Flag-Treslin/TICRR-WT, 2PM or ΔSTD were transiently transfected into 293T cells. Native lysates were used for anti-GFP nanobody immunoprecipitation (IP) in the presence of recombinant Cdk2-cyclin A to promote interaction with TopBP1. Lysates and bead-bound material were analysed by immunoblotting using mouse anti-GFP and rabbit anti-antibodies. Treslin/TICRR-2PM did not bind TopBP1, as expected because the relevant CDK sites in the TDIN are mutated to alanine. Treslin/TICRR- ΔSTD was able to bind to TopBP1.

(B) Independent experimental replicate of A.

Supplementary figure S5 –GFP-Treslin/TICRR-wild type (WT) and mutants used in this work retain their nuclear localisation. U2OS cells were transiently transfected with the indicated GFP-Flag-tagged Treslin/TICRR constructs used across this work (2PM, ΔSTD, ΔCIT, ΔC853, Core and ΔM2) to ascertain their cellular localisation. Cells were fixed with 2% PFA for 20 mins and stained with DAPI. Representative pictures of transfected cells are shown for each transfection. As can be seen by the juxtaposition with the DAPI channel, GFP signal in all conditions except the empty line localised to the nucleus, indicating that Treslin/TICRR-WT and all mutants tested retained nuclear localisation. Scale bar: 10 μM.

Supplementary figure S6 –AlphaFold models of Treslin/TICRR and MTBP

The AlphaFold structural models of Treslin/TICRR and MTBP suggest that their N-terminal regions share the same domain architecture, a vWA domain followed by a Ku70-like β-barrel, suggesting a common ancestry.

(A) Treslin/TICRR full length AlphaFold model showing the predicted vWA domain (blue), Ku70/80-like-β-barrel (red), STD domain (green), and the 518-543 region whose deletion abrogated MTBP binding (pink; AlphaFold prediction score < 70%).

(B) MTBP full length AlphaFold model showing the predicted vWA (blue), Ku70-like β-barrel (red) and S7MC domain (grey).

Supplementary figure S7 – The CIT domain of Treslin/TICRR contains a vWA fold

Representative multiple sequence alignment of VWA domain in Treslin/TICRR family. Secondary structure prediction using PsiPred was performed for the Treslin/TICRR family, shown in the first lane; this prediction is consistent with the secondary structure of VWA domains, shown below each of the selected proteins with known structure (CFB, PDB:3HRZD; Sec23, PDB:2NUTA; Ku70, PDB:5Y58E). For figure methods and abbreviations see Figure 2A legend.

Supplementary figure S8 – Structural similarities among Treslin/TICRR, MTBP, and Ku70 proteins.

(A) Contact maps of Ku70-like β-barrel domains of Treslin/TICRR (Alphafold model), Ku70 (PDB:5Y58_A), Sld7 (PDB:3x37_B), and Sld3 (PDB:3x37_A). Contact maps were generated using the Cocomaps server (cut-off distance value = 7 Å) (Vangone et al 2011). β-strands are labelled 1 to 7 and coloured in red, orange, yellow, green, cyan, violet, and purple, respectively. β-strand contact pairs are labelled, showing the identical arrangement of the seven β-strands conserved among these Ku70-like β-barrel domains. In Sld3 the β-barrel is incomplete, missing β strands 1 and 2 (Ku70 barrel numbering).

(B) Dali structural superposition of the vWA domains of human Treslin/TICRR (Treslin/TICRR Alphafold model positions 1 to 250 in green), human MTBP (MTBP Alphafold model positions 1 to 236 in cyan; Z-score 9.6 and RMSD 3.6Å versus Treslin/TICRR), and yeast Ku70

(PDB: 5y58-A, positions 28 to 263 in purple; Z-score 10 and RMSD 3.8Å versus Treslin/TICRR).

(C) Dali structural superposition of the β-barrel domains of human Treslin/TICRR (Treslin/TICRR alphafold model position 299 to 424 in green), human MTBP (MTBP alphafold model positions 237 to 420 in cyan; Z-score 10.1 and RMSD 3.4Å versus Treslin/TICRR), and yeast Ku70 (PDB: 5y58-A, positions 264 to 451 in purple; Z-score 13.3 and RMSD 2.6Å versus Treslin/TICRR).

Supplementary figure S9 – Mutating individual β-strands from Treslin/TICRR β-barrel compromises binding to MTBP

(A) Treslin/TICRR alphafold model showing the β-barrel (red), including the three β-strands mutated in B. β-strand 1 (amino acids 391 to 396, HLVADV, replaced with amino acids SGELRL, labeled in yellow), β-strand 2 (amino acids 405 to 412, ITGVISPL, replaced with amino acids SGELRLPS, labeled in blue), or β-strand 3 (amino acids 415 to 423, SAMILTVCR, replaced with amino acids LLCIKVEAF, labeled in green).

(B) N-terminally 3HA-tagged Treslin/TICRR fragments (from amino acid 260 to 671) were transiently transfected into 293T together with C-terminally GFP-tagged MTBP before immunoprecipitation from cell lysates using anti-GFP nanobody immunoprecipitation (IP). The Treslin/TICRR fragments used were wild type (WT), β-strand 1m (labeled in yellow in A), β-strand 2m (labeled in blue in A), or β-strand 3m (labeled in green in A). The Treslin/TICRR β-strand amino acids were replaced by unrelated β-strand forming sequences, in order to try to change the amino acid sequence without disrupting the overall structure. Results show that each β-strand mutation weakened but did not abrogate binding to MTBP, indicating that each individual β-strand may contribute to the MTBP interaction surface.

Supplementary figure S10 – Analysis of several stable U2OS clones expressing Treslin/TICRR-ΔCIT or various C-terminal truncation mutants.

A) Schematic giving an overview over the Treslin/TICRR mutants used in this figure.

B-D) Immunoblots (i) to assess transgene expression levels and BrdU-flow cytometry (ii) and PI profiles (iii) to determine overall DNA replication of the indicated Treslin/TICRR mutants shown in A. The following U2OS clones were used for main Fig 4: Treslin/TICRR-ΔCIT-5, ΔC853-5. Immunoblots of whole cell lysates used mouse anti-GFP and Ponceau staining (as a loading control). Flow cytometry was done after replacing endogenous Treslin/TICRR against the indicated siRNA-resistant transgenes using RNAi. Density plots are shown. Parental U2OS cells and a line expressing Treslin/TICRR-WT served to control the experiment. Dashed lines show BrdU peak level of the respective control siRNA-treated cell line in the same experiment. Clones were picked that expressed the Treslin/TICRR transgenes at similar or higher levels than Treslin/TICRR-WT to avoid under-estimating the capability of the mutants to support replication. For Treslin/TICRR-ΔC651, only low-expressing clones were found. The results are still conclusive, though, because all clones were capable to support replication.

E) Quantification of overall replication in mutant Treslin/TICRR U2OS cell lines described in A-D, based on BrdU-PI flow cytometry experiments as described in B-D. For comparison, the Treslin/TICRR-core clones are shown in addition to the usual control lines. The quantifications indicate that ΔCIT, ΔC651 and ΔC853 mutants were active. It also shows the clonal variability that did not clearly correlate with expression levels, as indicated by the Treslin/TICRR-ΔC651 clones 1-3. Error bars: SEM; sample numbers (n): 8 (none; WT), 5

(ΔCIT-5; ΔC853-5), 4(ΔCIT-7); 3 (ΔC651-2; ΔC651-3; ΔC651-38; ΔC853-29, core-35; core-41); 2 (ΔC853-13); significance tests: parametric, unpaired, two tailed student t-test, *P≤0.05.

Supplementary figure S11 – Analysis of several stable U2OS clones expressing Treslin/TICRR-core and Treslin/TICRR-ΔCIT/ΔC651

A) Schematic giving an overview over the Treslin/TICRR mutants used in B-E

B-D) Immunoblots (B) and BrdU-Flow cytometry/PI profiles (C/D) of stable U2OS cell lines expressing indicated Treslin/TICRR-mutants shown in A. Immunoblots of whole cell lysates using mouse anti-GFP and Ponceau staining (as a loading control) served to assess transgene expression levels relative to each other and Treslin/TICRR-WT. The following U2OS clones were used for main figures: Treslin/TICRR-ΔCIT/ΔC651-61 (Fig 4), core-35 (Fig 4, 5). Clones were picked that expressed the Treslin/TICRR transgenes at similar or higher levels than Treslin/TICRR-WT to avoid under-estimating the capability of the mutants to support replication. For BrdU-flow cytometry, density plots show overall DNA replication of stable U2OS clones shown in A. Flow cytometry was done after replacing endogenous Treslin/TICRR against the indicated siRNA-resistant transgenes using RNAi. Parental U2OS cells and a line expressing Treslin/TICRR-WT served to control the experiment. Dashed lines show BrdU peak level of the respective control siRNA-treated cell line in the same experiment.

E) Quantification of overall replication in mutant Treslin/TICRR U2OS cell lines described in A, based on BrdU-PI flow cytometry experiments as described in B. For comparison, Treslin/TICRR-ΔCIT containing the full C-terminus and Treslin/TICRR-core are shown in addition to the usual control lines. Treslin/TICRR-ΔCIT/ΔC651 supports replication to levels comparable with Treslin/TICRR-ΔCIT. The exact level of replication depended on the clone

1087 used. No Treslin/TICRR-ΔCIT/ΔC651 clone, however, supported replication as poorly as
1088 Treslin/TICRR-core that showed replication similar to control U2OS cells not expressing a
1089 siRNA-resistant transgene. Error bars: SEM; sample numbers (n): 8 (none; WT), 5 (ΔCIT(-C-
1090 full)-5;), 4 (ΔCIT(-C-full)-7), 3 (ΔCIT-ΔC651-57; ΔCIT-ΔC651-61; core-35; core-41);
1091 significance tests: parametric, unpaired, two tailed student t-test, *P≤0.05.
1092
1093 **Supplementary figure S12 – Analysis of several stable U2OS clones expressing various C-**
1094 **terminal truncations in combination with deletion of the CIT or Treslin/TICRR-ΔC99**
1095 **A)** Schematic giving an overview over the Treslin/TICRR mutants used in B-E.
1096 **B/C/D)** Immunoblots (i) to assess transgene expression levels of stable U2OS clones
1097 expressing Treslin/TICRR-ΔCIT/ΔC651 and ΔCIT/ΔC853. Immunoblots of whole cell lysates
1098 used mouse anti-GFP and Ponceau staining (as a loading control). Clones were picked that
1099 expressed the Treslin/TICRR transgenes at similar or higher levels than Treslin/TICRR-WT to
1100 avoid under-estimating the capability of the mutants to support replication. Density plots (ii)
1101 of BrdU-flow cytometry and PI profiles (iii) to determine overall DNA replication of stable
1102 U2OS clones described in A and B. Flow cytometry was done after replacing endogenous
1103 Treslin/TICRR against the indicated siRNA-resistant transgenes using RNAi. Parental U2OS
1104 cells and a line expressing Treslin/TICRR-WT served to control the experiment. Dashed lines
1105 show BrdU peak level of the respective control siRNA-treated cell line in the same
1106 experiment.
1107 **E)** Quantification of overall replication in mutant Treslin/TICRR U2OS cell lines described in
1108 A, based on BrdU-PI flow cytometry experiments as described in B. For comparison,
1109 Treslin/TICRR-ΔCIT containing the full C-terminus and Treslin/TICRR-core are shown in
1110 addition to the usual control lines. Treslin/TICRR-ΔC99 supports replication to similar levels

as Treslin/TICRR-WT. Treslin/TICRR-ΔCIT/ΔC99 supports replication to levels comparable with Treslin/TICRR-ΔCIT, but much better than Treslin/TICRR-core. Also here, the exact level of replication depended on the clone used. Error bars: SEM; sample numbers (n): 8 (none; WT), 5 (ΔCIT(-C-full)-5;), 4 (ΔCIT(-C-full)-7), 3 (ΔC-99-4; ΔCIT-ΔC99-25; ΔCIT-ΔC309-9; ΔCIT-ΔC309-20; ΔCIT-ΔC394-13; ΔCIT-ΔC394-15; core-35; core-41); significance tests: parametric, unpaired, two tailed student t-test, *P≤0.05.

Supplementary figure S13 – Treslin/TICRR-core is proficient in binding MTBP and TopBP1

(A) The indicated GFP-Flag-Treslin/TICRR mutants were transiently transfected into 293T cells together with MTBP. Native lysates were used for anti-GFP nanobody immunoprecipitation (IP) in the presence of recombinant Cdk2-cyclin A to promote interaction with TopBP1. Lysates and bead-bound material were analysed by immunoblotting using mouse anti-GFP, rabbit anti-TopBP1 and rat anti-MTBP antibodies. Controls for IP specificity were made: Treslin/TICRR-ΔM1 and ΔM2 show decreased (M1) or absent (M2) MTBP signals, as expected. Treslin/TICRR-2PM did not bind TopBP1, as expected because the relevant CDK sites in the TDIN are mutated to alanine. IP capabilities using (near) full-length Treslin/TICRR versions are hard to compare by immunoblotting with those containing larger deletions because of the often weak blotting efficiency of the 210 kD full-length Treslin/TICRR. However, the smaller C-terminal truncations are better comparable. Treslin/TICRR-ΔC853 and Δ651 bound similar amounts of TopBP1 and MTBP, whether they contained CIT or not. In some experiments, however, deletion of the CIT seemed to have a minor effect on the amount of MTBP bound (Fig 4D).

(B) Independent experimental replicate of A, containing only some key samples.

Figure 1

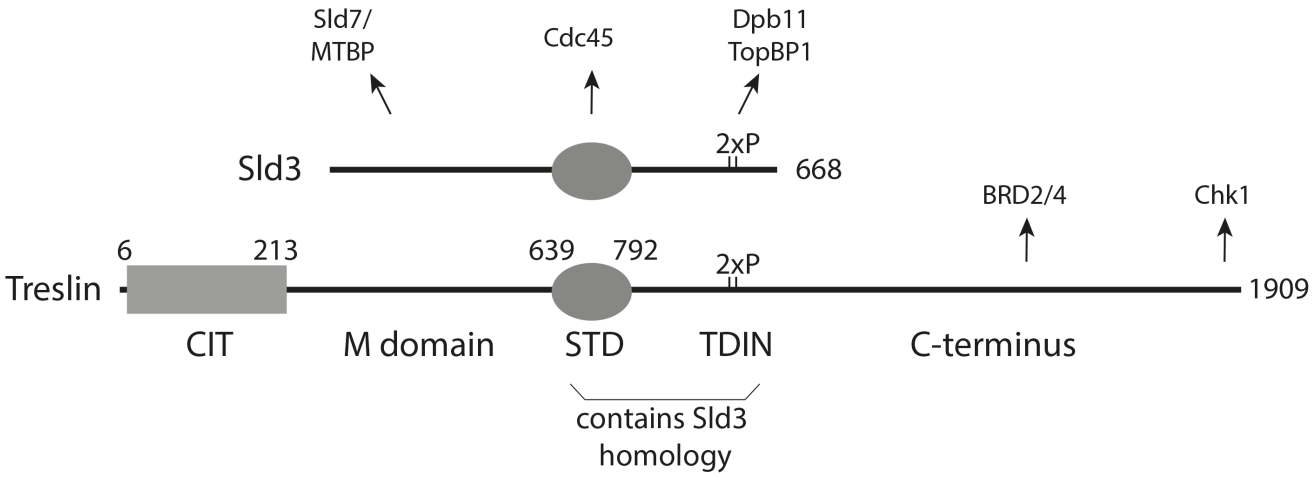
Sld7/
MTBP
Cdc45
Dpb11
TopBP1
Sld3
2xP
668
BRD2/4
Chk1
6
213
639
792
2xP
Treslin
1909
CIT
M domain
STD
TDIN
C-terminus
contains Sld3
homology

Figure 2

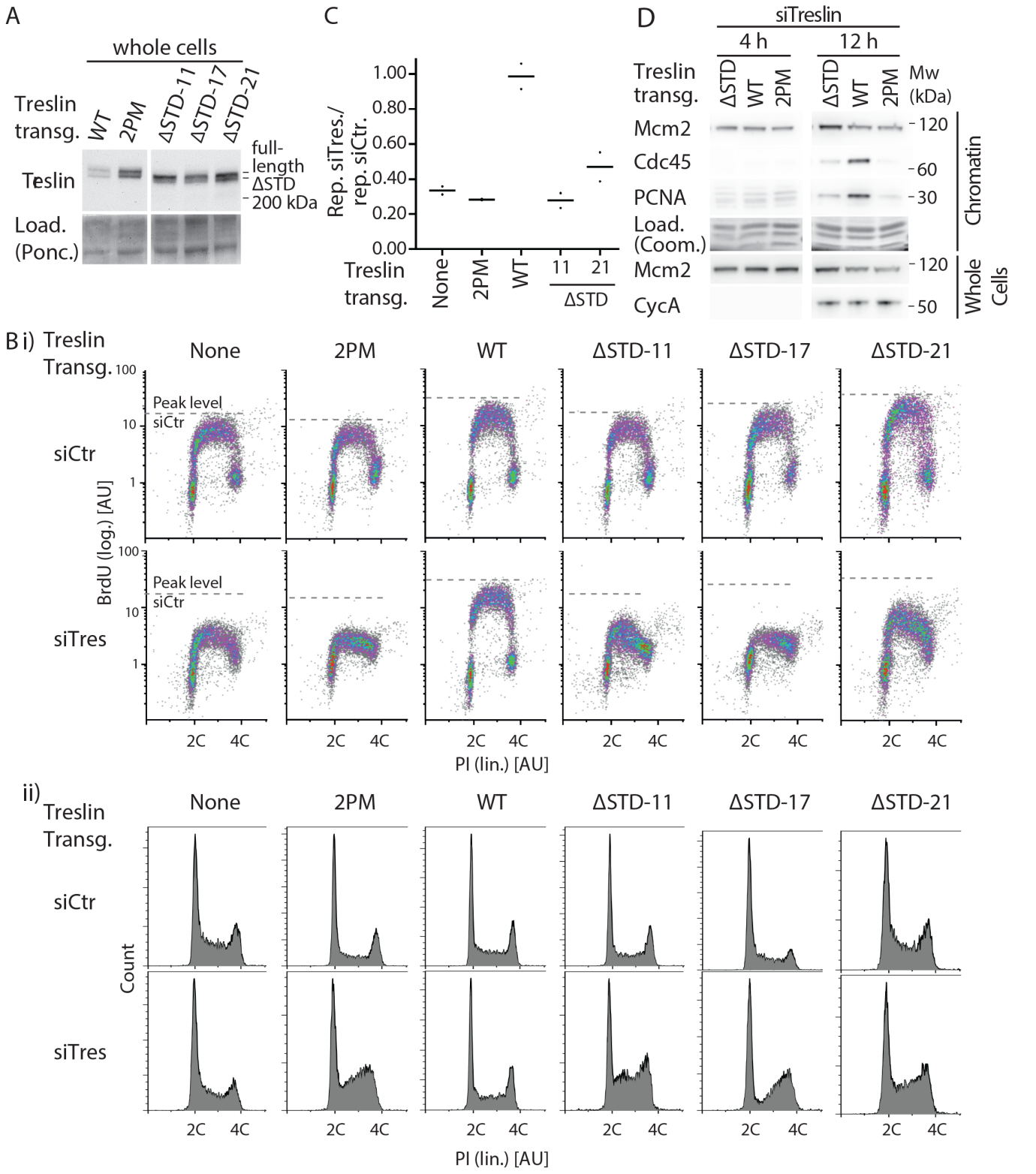
A
whole cells
Treslin transg.
WT
2PM
ΔSTD-11
ΔSTD-17
ΔSTD-21
Treslin
full-length
ΔSTD
200 kDa
Load. (Ponc.)
C
Rep. siTres./ rep. siCtr.
1.00
0.80
0.60
0.40
0.20
0.00
Treslin transg.
None
2PM
WT
11
21
ΔSTD
D
siTreslin
4 h
12 h
Treslin transg.
ΔSTD
WT
2PM
Mw (kDa)
Mcm2
Cdc45
PCNA
Load. (Coom.)
120
60
30
Chromatin
Mcm2
CycA
120
50
Whole Cells
B i) Treslin Transg.
None
2PM
WT
ΔSTD-11
ΔSTD-17
ΔSTD-21
siCtr
siTres
Peak level siCtr
BrdU (log.) [AU]
100
10
1
2C
4C
PI (lin.) [AU]
ii)
Count

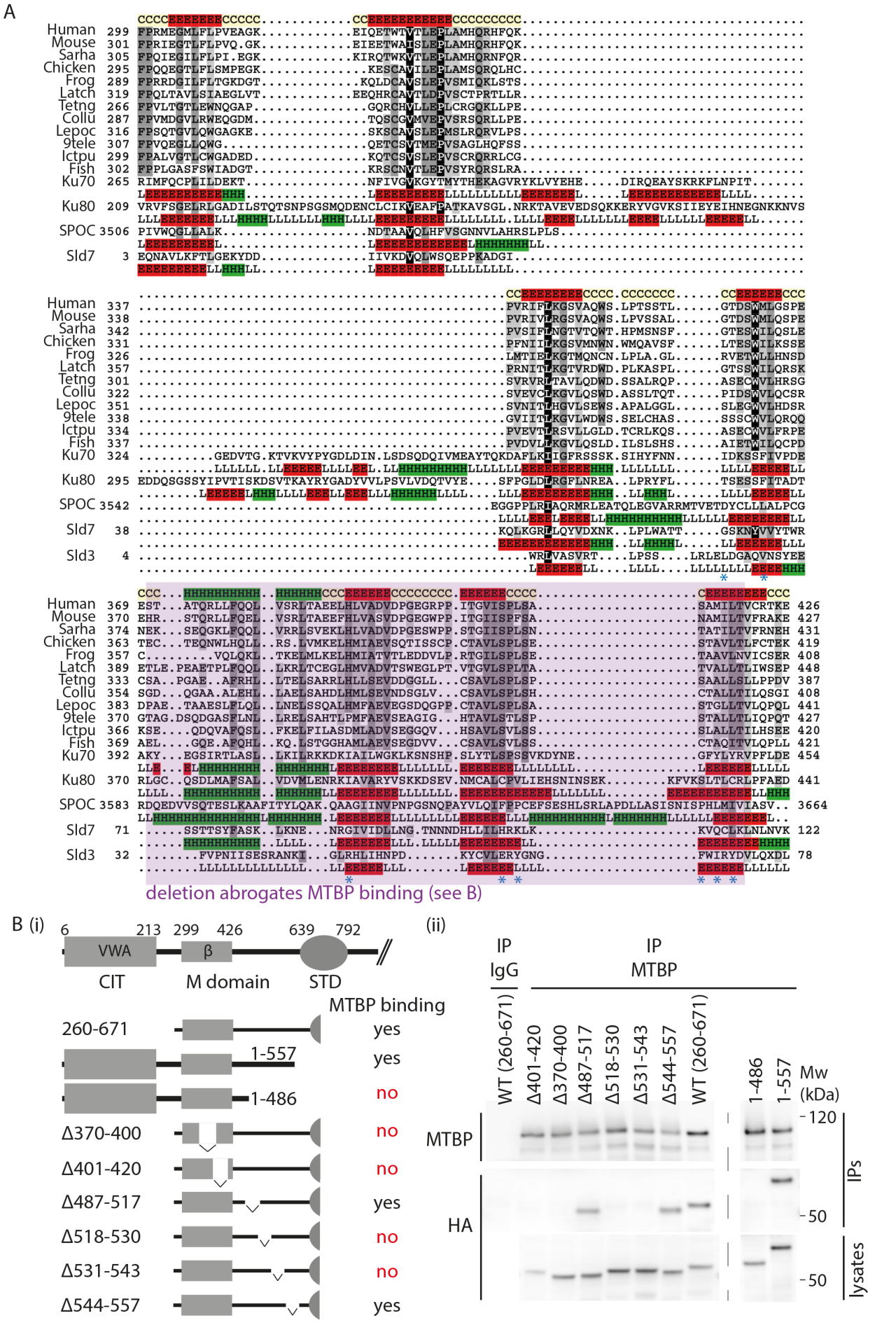
A
Human
Mouse
Sarha
Chicken
Frog
Latch
Tetng
Collu
Lepoc
9tele
Ictpu
Fish
Ku70
Ku80
SPOC
Sld7
Sld3
deletion abrogates MTBP binding (see B)
B (i)
6
213
299
426
639
792
VWA
β
CIT
M domain
STD
MTBP binding
260-671
yes
1-557
yes
1-486
no
Δ370-400
no
Δ401-420
no
Δ487-517
yes
Δ518-530
no
Δ531-543
no
Δ544-557
yes
(ii)
IP IgG
IP MTBP
WT (260-671)
Δ401-420
Δ370-400
Δ487-517
Δ518-530
Δ531-543
Δ544-557
WT (260-671)
1-486
1-557
Mw (kDa)
120
50
50
MTBP
HA
IPs
lysates

Figure 4

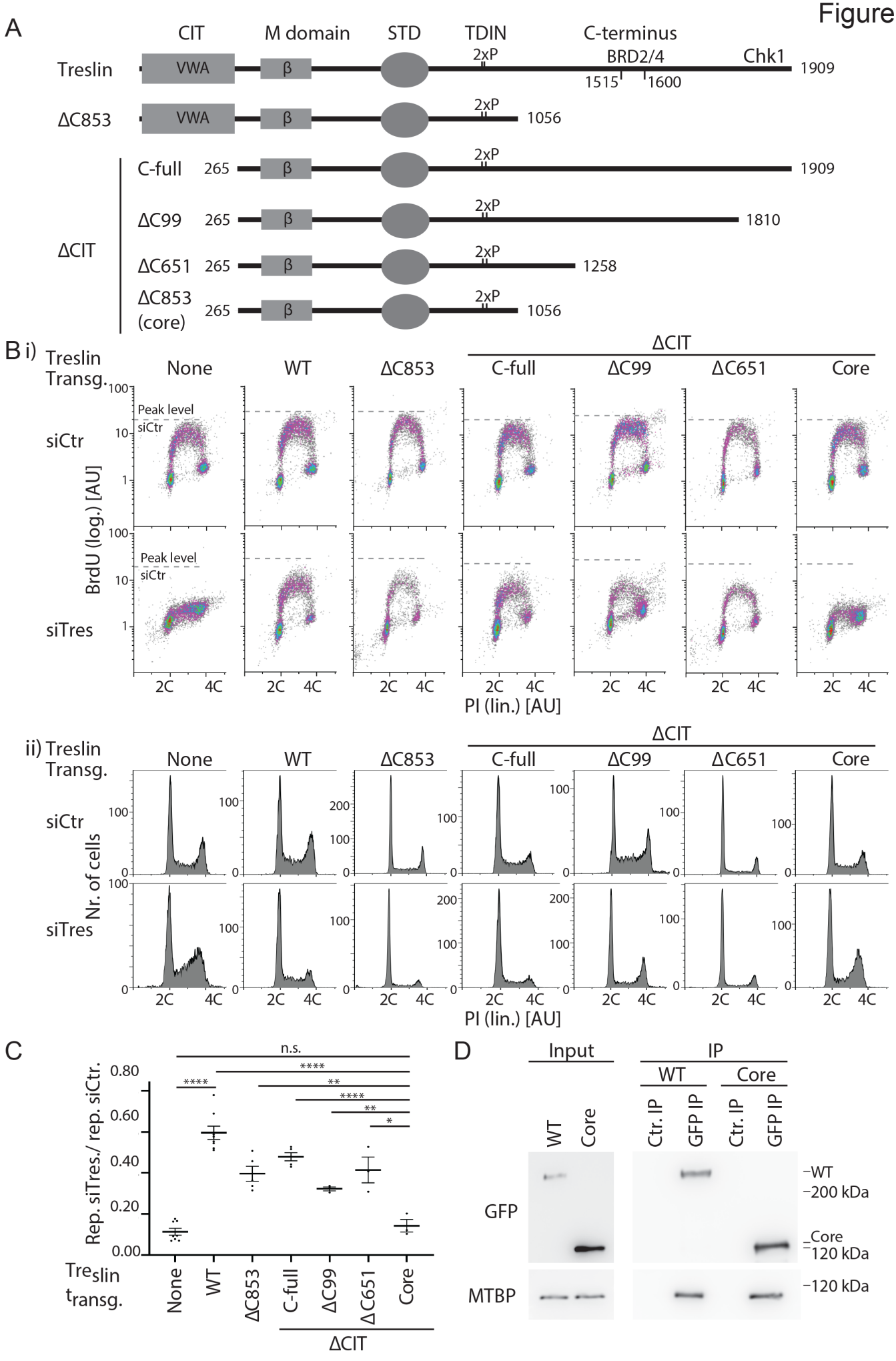
A
CIT
M domain
STD
TDIN
C-terminus
Treslin
VWA
β
2xP
BRD2/4
Chk1
1515
1600
1909
ΔC853
1056
ΔCIT
C-full
265
ΔC99
1810
ΔC651
1258
ΔC853 (core)
B i)
Treslin Transg.
None
WT
ΔC853
ΔCIT
C-full
ΔC99
ΔC651
Core
siCtr
siTres
Peak level siCtr
BrdU (log.) [AU]
PI (lin.) [AU]
2C
4C
ii)
Nr. of cells
C
Rep. siTres./ rep. siCtr.
n.s.
****
**
*
Treslin transg.
D
Input
IP
WT
Core
Ctr. IP
GFP IP
GFP
MTBP
WT
200 kDa
Core
120 kDa

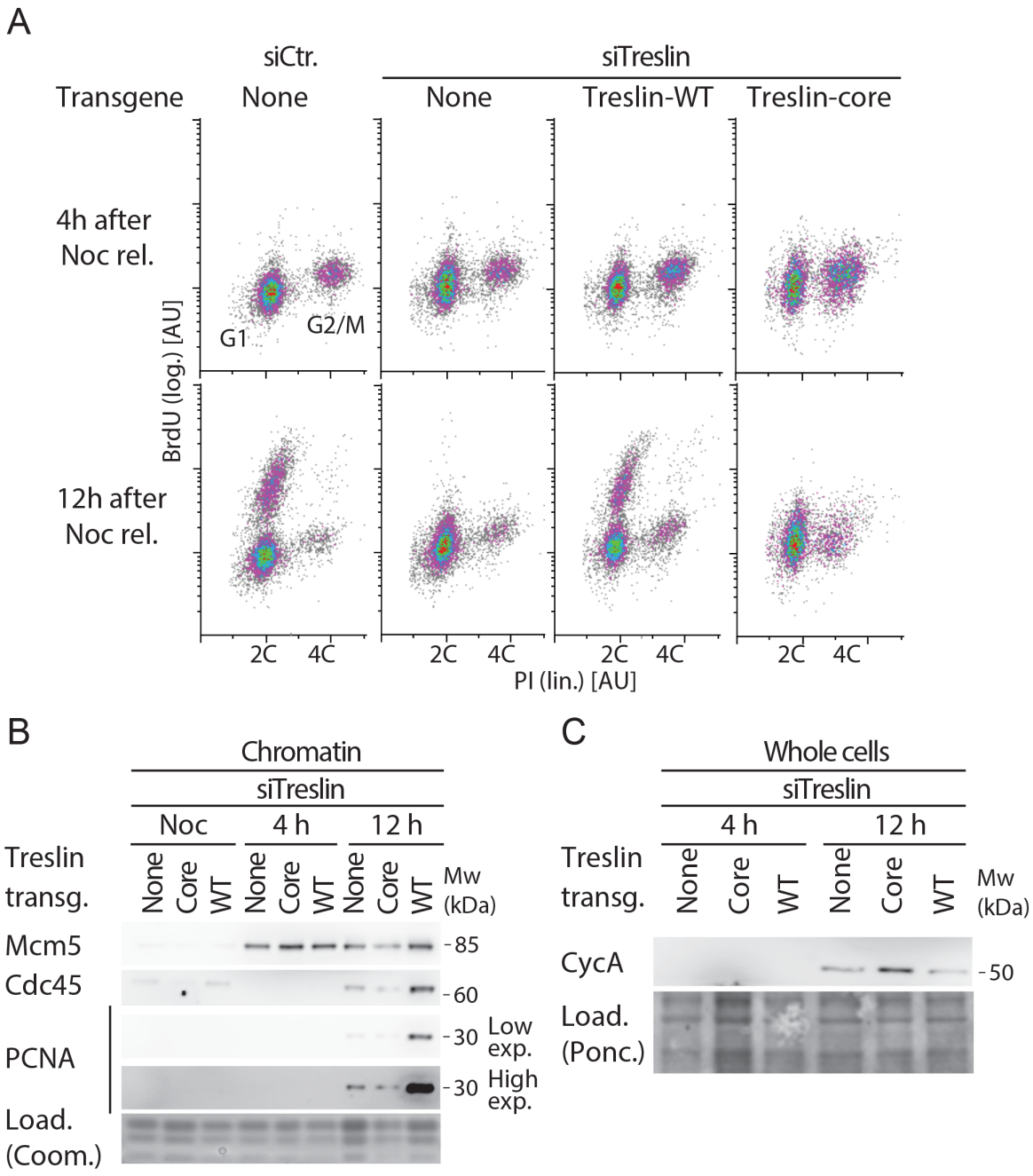
A
siCtr.
siTreslin
Transgene
None
None
Treslin-WT
Treslin-core
4h after Noc rel.
12h after Noc rel.
BrdU (log.) [AU]
G1
G2/M
2C
4C
PI (lin.) [AU]
B
Chromatin
siTreslin
Noc
4 h
12 h
Treslin transg.
None
Core
WT
Mw (kDa)
Mcm5
Cdc45
PCNA
Load. (Coom.)
85
60
30
Low exp.
High exp.
C
Whole cells
siTreslin
4 h
12 h
CycA
Load. (Ponc.)
50

Figure 6

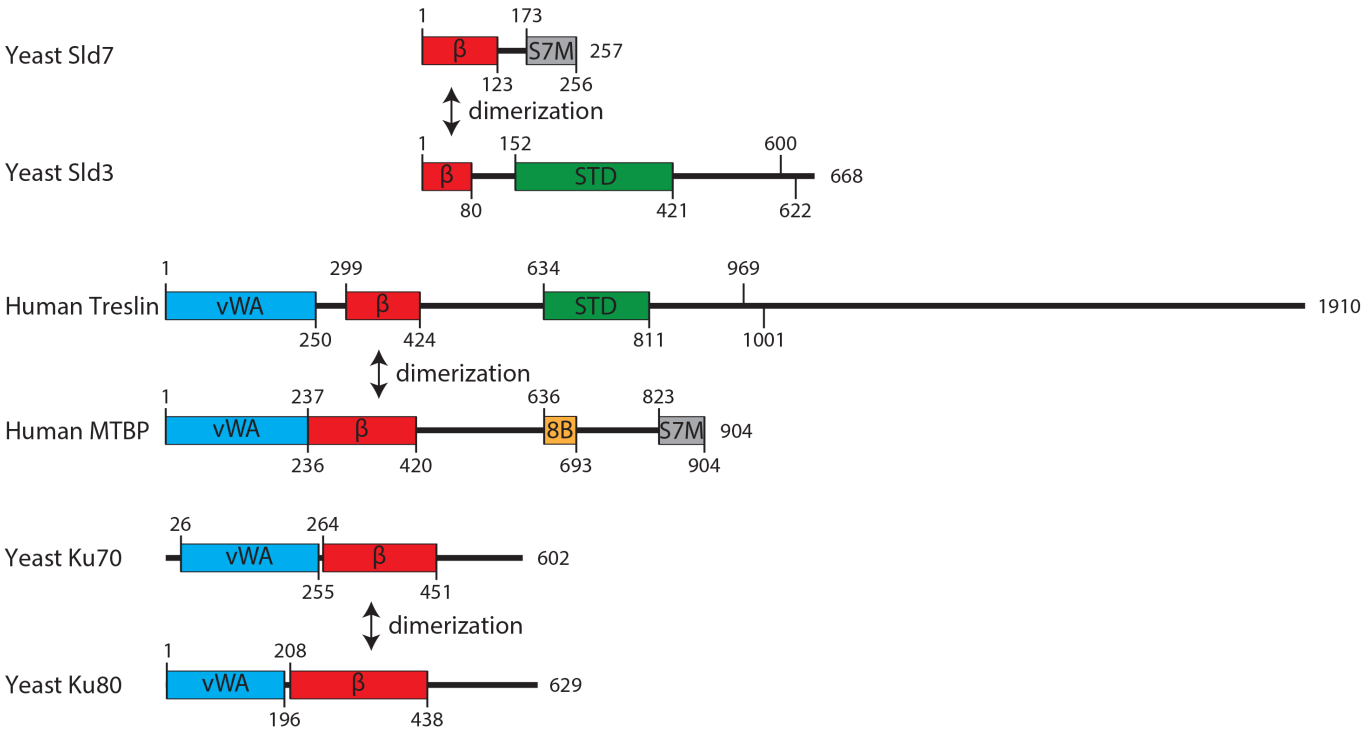
Yeast Sld7
1
173
β
S7M
257
123
256
dimerization
Yeast Sld3
1
152
600
β
STD
668
80
421
622
Human Treslin
1
299
634
969
vWA
β
STD
1910
250
424
811
1001
dimerization
Human MTBP
1
237
636
823
vWA
β
8B
S7M
904
236
420
693
904
Yeast Ku70
26
264
vWA
β
602
255
451
dimerization
Yeast Ku80
1
208
vWA
β
629
196
438

Figure S1

A

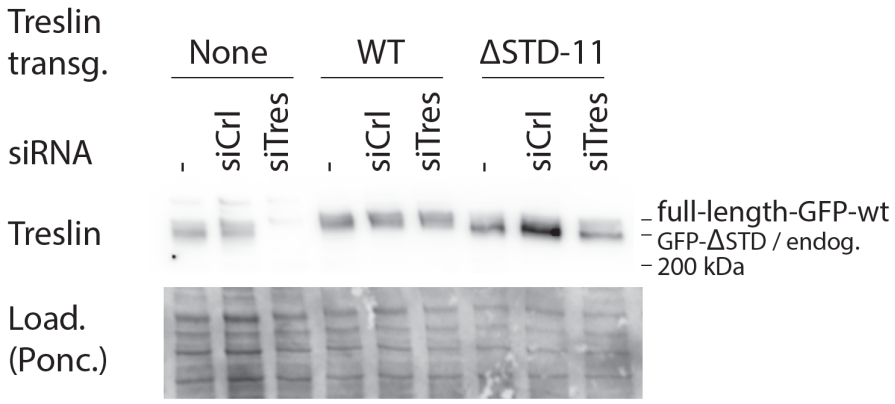
Treslin transg.
None
WT
ΔSTD-11
siRNA
-
siCrl
siTres
-
siCrl
siTres
-
siCrl
siTres
Treslin
full-length-GFP-wt
GFP-ΔSTD / endog.
200 kDa
Load. (Ponc.)

B

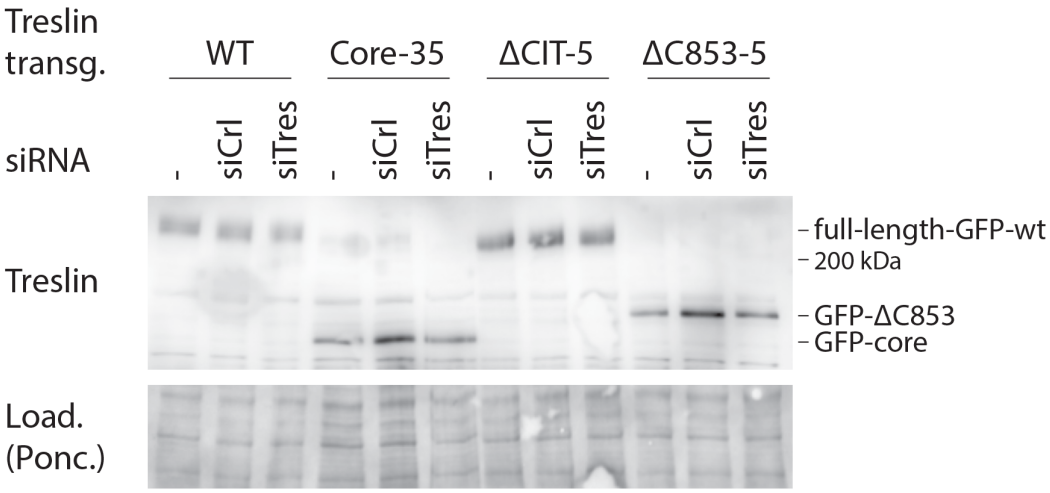
Treslin transg.
WT
Core-35
ΔCIT-5
ΔC853-5
siRNA
-
siCrl
siTres
-
siCrl
siTres
-
siCrl
siTres
-
siCrl
siTres
Treslin
full-length-GFP-wt
200 kDa
GFP-ΔC853
GFP-core
Load. (Ponc.)

Figure S2

A Ungated data

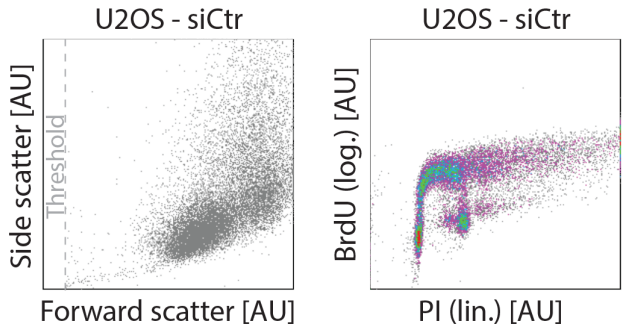

B Doublet discrimination

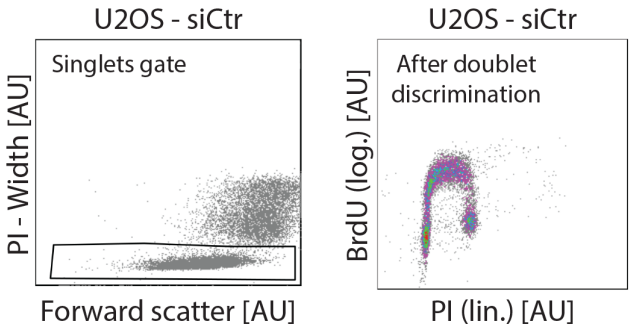

C Gating of S-phase cells (BrdU positive) and cells outside of S-phase (BrdU negative)

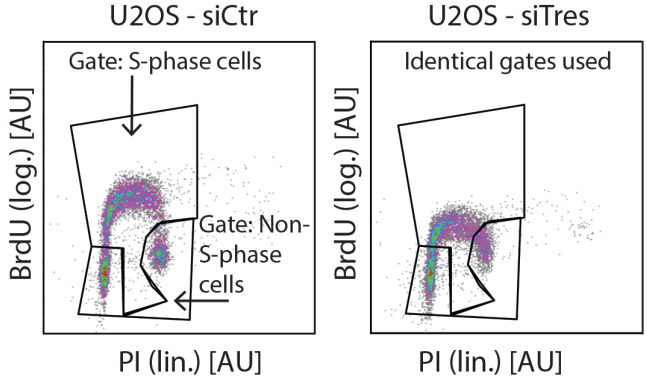

Average BrdU signal intensity [AU]:

U2OS - siCtr	U2OS - siTres
S-phase cells: 5.98	S-phase cells: 2.73
Non-S-phase cells: 0.90	Non-S-phase cells: 0.91

D Calculating BrdU dependent replication signal

Average BrdU dependent replication signal =
S-phase cells intensity - Non-S-phase cells intensity

U2OS-siCtr BrdU dependent replication:
5.98 - 0.90 = 5.08 [AU]

U2OS-siTres BrdU dependent replication:
2.73 - 0.91 = 1.82 [AU]

E Quantification of relative replication of siTreslin treated cells normalised to siCtr treaded cells

Replication siTres / Replication siCtr
1.82 / 5.08 = 0.36

Replication rescue: siTrestlin treated cells incorporated 36% of BrdU in comparison to siCtrl treated cells

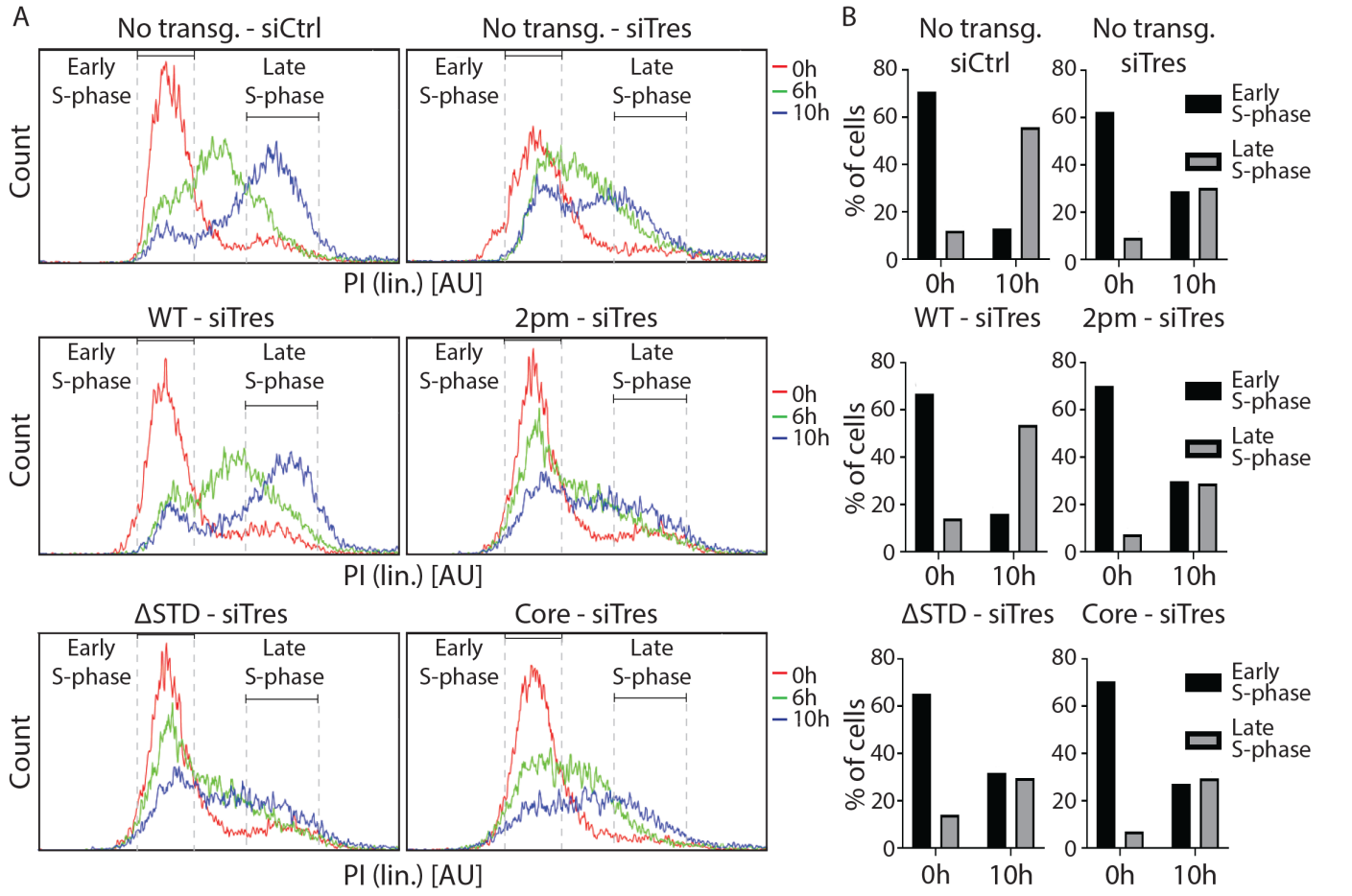
A
No transg. - siCtrl
No transg. - siTres
WT - siTres
2pm - siTres
ΔSTD - siTres
Core - siTres
Early S-phase
Late S-phase
Count
PI (lin.) [AU]
0h
6h
10h
B
% of cells
Early S-phase
Late S-phase
0h
10h

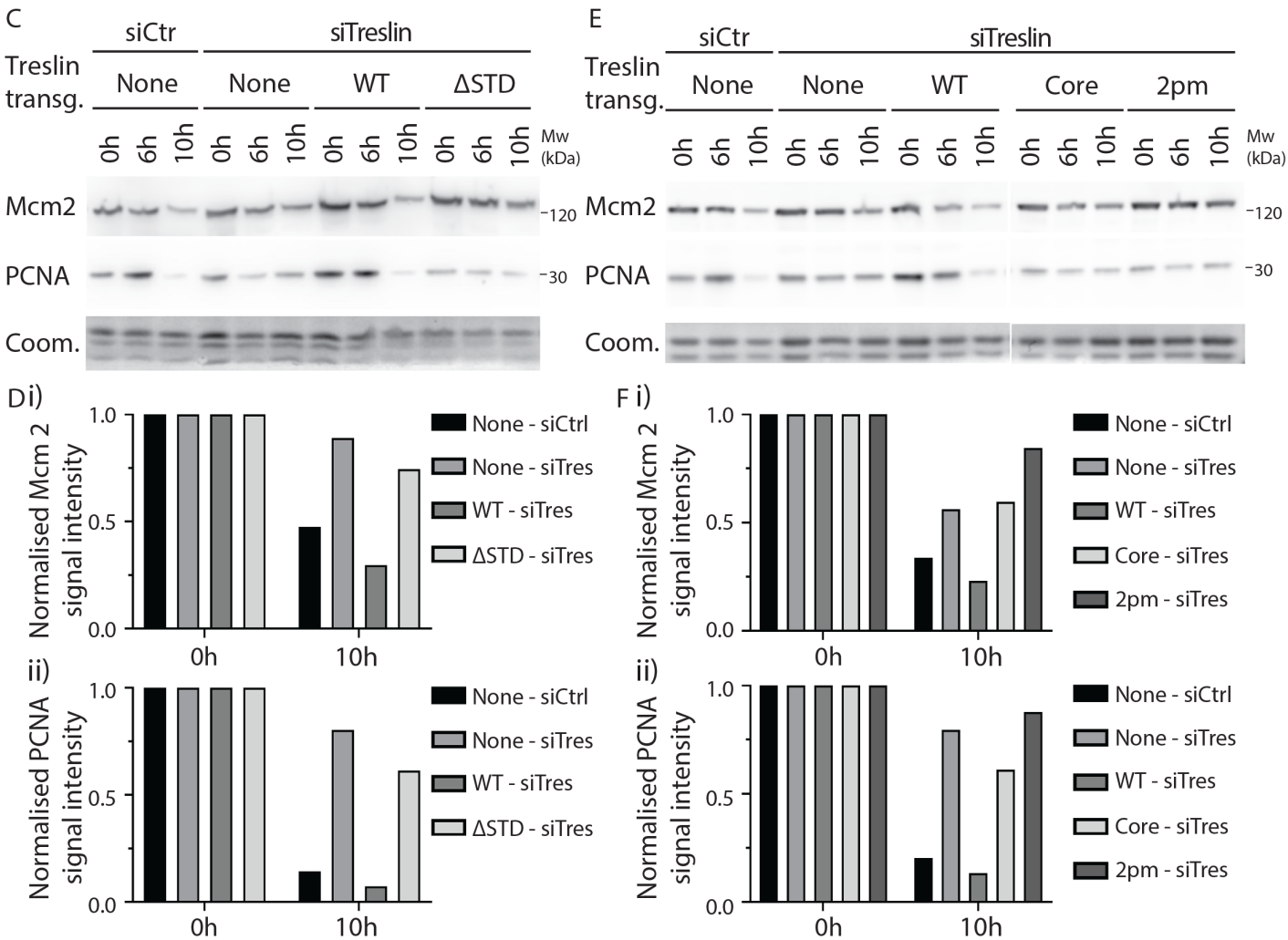
C
siCtr
siTreslin
Treslin transg.
None
None
WT
ΔSTD
0h
6h
10h
Mw (kDa)
Mcm2
PCNA
Coom.
120
30
E
siCtr
siTreslin
Treslin transg.
None
None
WT
Core
2pm
Di)
ii)
Normalised Mcm 2 signal intensity
Normalised PCNA signal intensity
1.0
0.5
0.0
0h
10h
None - siCtrl
None - siTres
WT - siTres
ΔSTD - siTres
F i)
ii)
Core - siTres
2pm - siTres

Figure S4

A

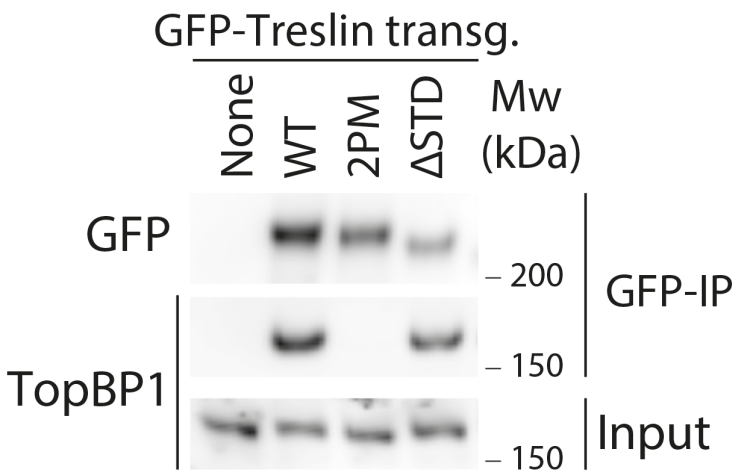
GFP-Treslin transg.
None
WT
2PM
ΔSTD
Mw (kDa)
GFP
TopBP1
– 200
– 150
– 150
GFP-IP
Input

B

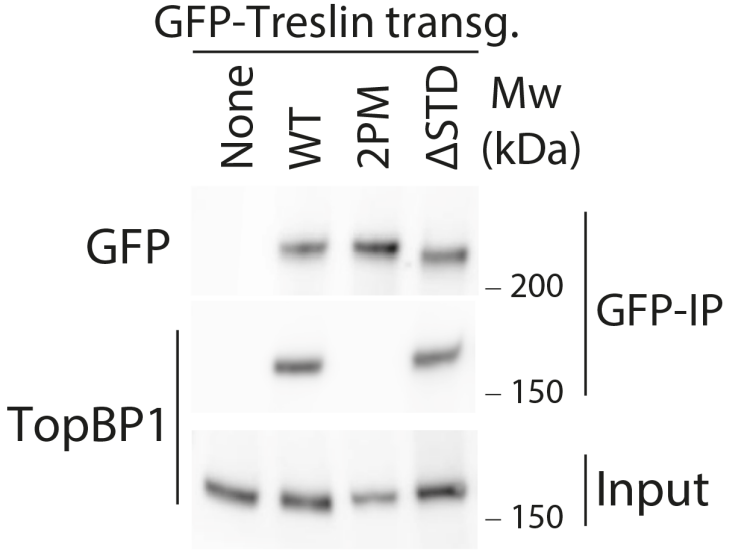
GFP-Treslin transg.
None
WT
2PM
ΔSTD
Mw (kDa)
GFP
TopBP1
– 200
– 150
– 150
GFP-IP
Input

Figure S5

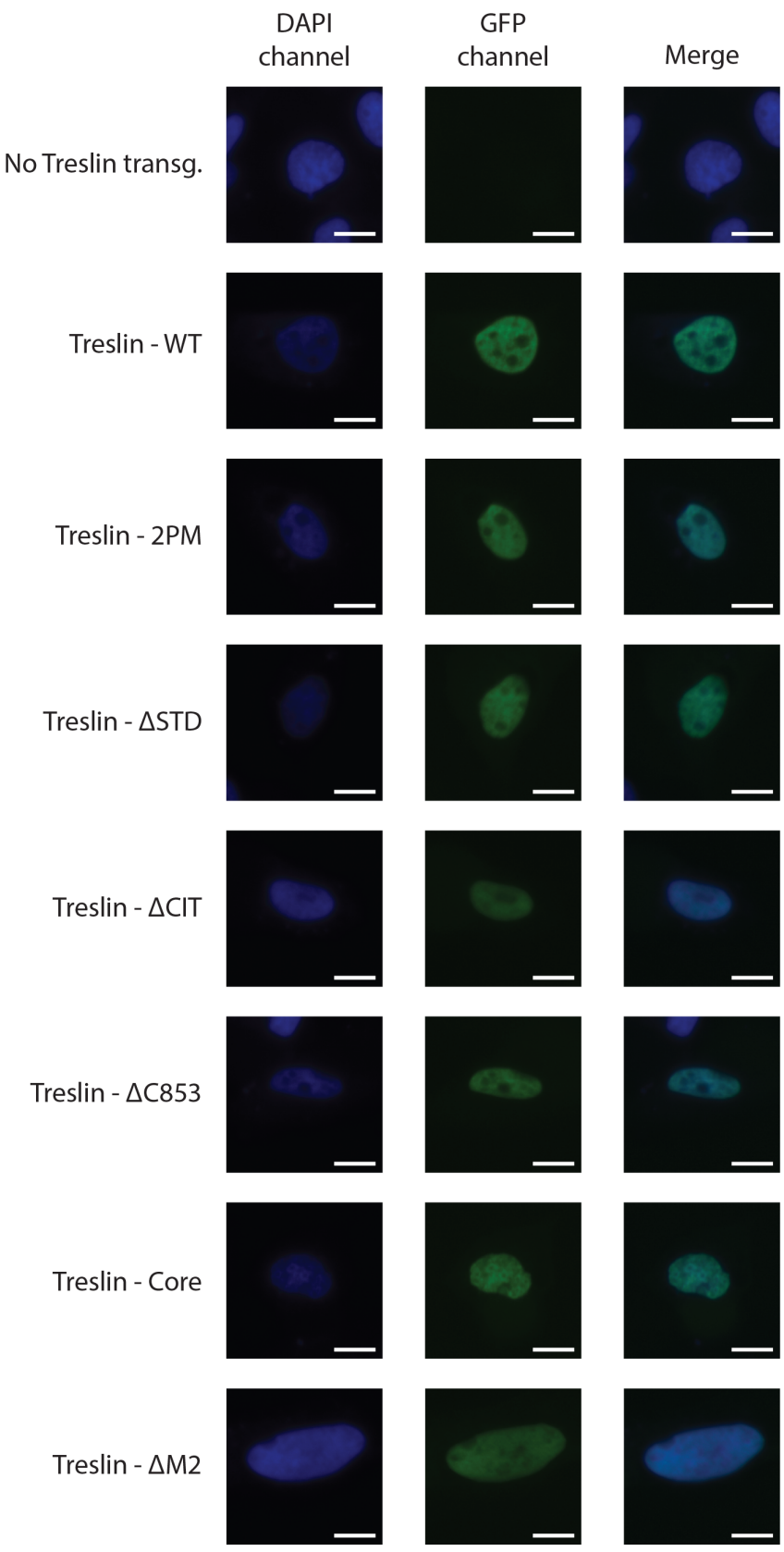
DAPI channel
GFP channel
Merge
No Treslin transg.
Treslin - WT
Treslin - 2PM
Treslin - ΔSTD
Treslin - ΔCIT
Treslin - ΔC853
Treslin - Core
Treslin - ΔM2

Figure S6

A

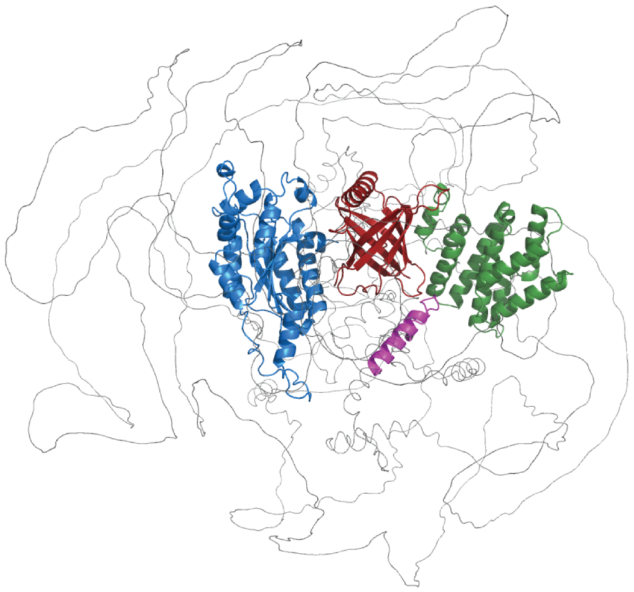

Legend:

vWA domain
β-barrel
518-543 region
STD domain

B

Legend:

vWA domain
β-barrel
S7MC domain

Figure S7

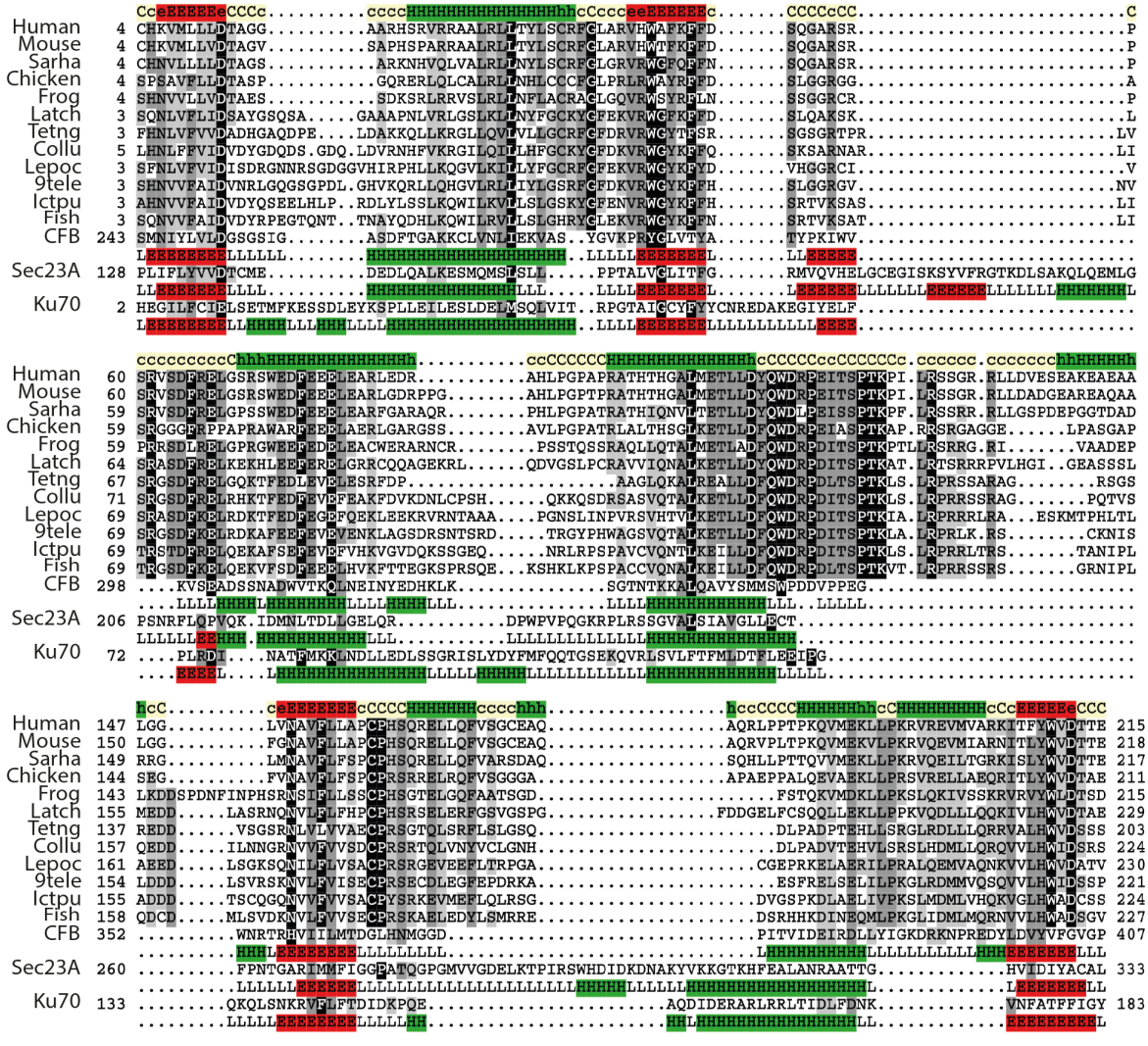
Human
Mouse
Sarha
Chicken
Frog
Latch
Tetng
Collu
Lepoc
9tele
Ictpu
Fish
CFB
Sec23A
Ku70

Figure S8

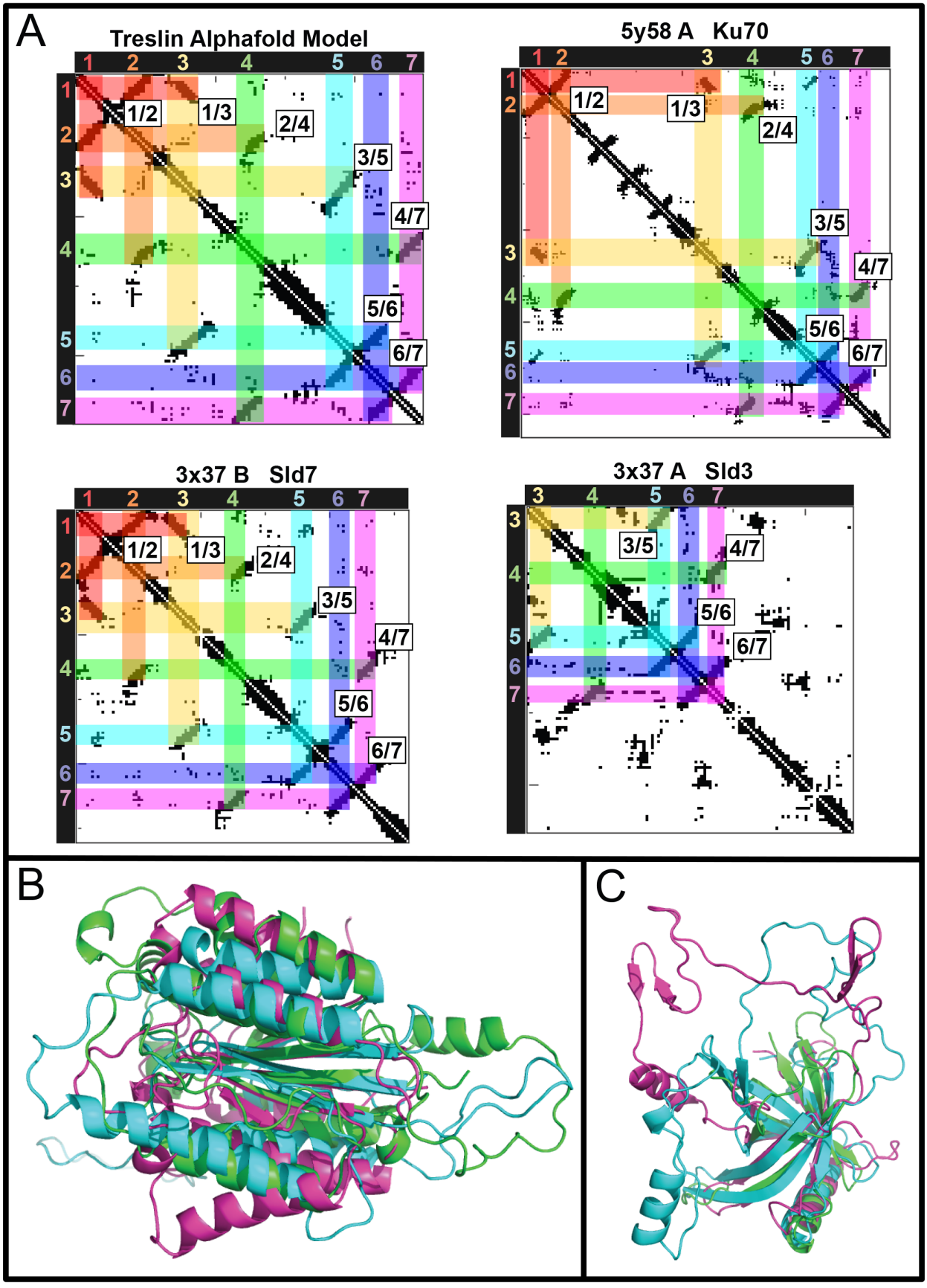
A
Treslin Alphafold Model
1 2 3 4 5 6 7
1/2
1/3
2/4
3/5
4/7
5/6
6/7
5y58 A Ku70
1 2 3 4 5 6 7
1/2
1/3
2/4
3/5
4/7
5/6
6/7
3x37 B Sld7
1 2 3 4 5 6 7
1/2
1/3
2/4
3/5
4/7
5/6
6/7
3x37 A Sld3
3 4 5 6 7
3/5
4/7
5/6
6/7
B
C

Figure S9

A

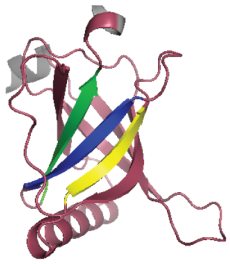

Legend:

β-barrel
β-strand 1: HLVADV
β-strand 2: ITGVISPL
β-strand 3: SAMILTVCR

B

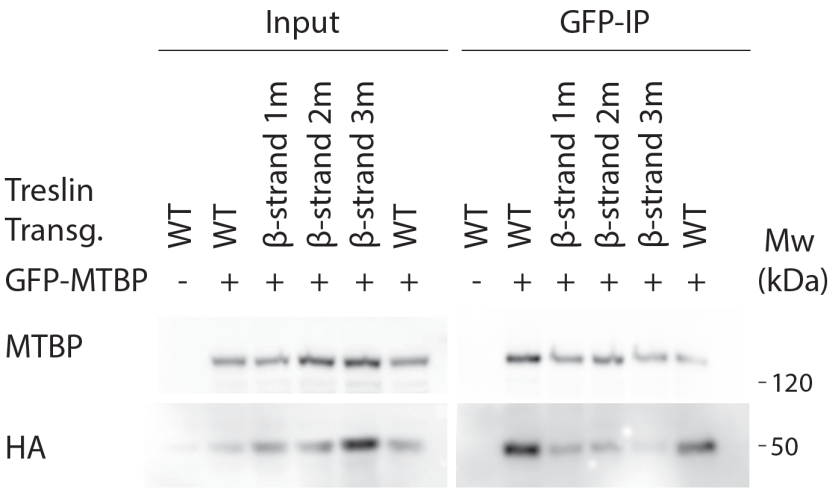

Figure S10

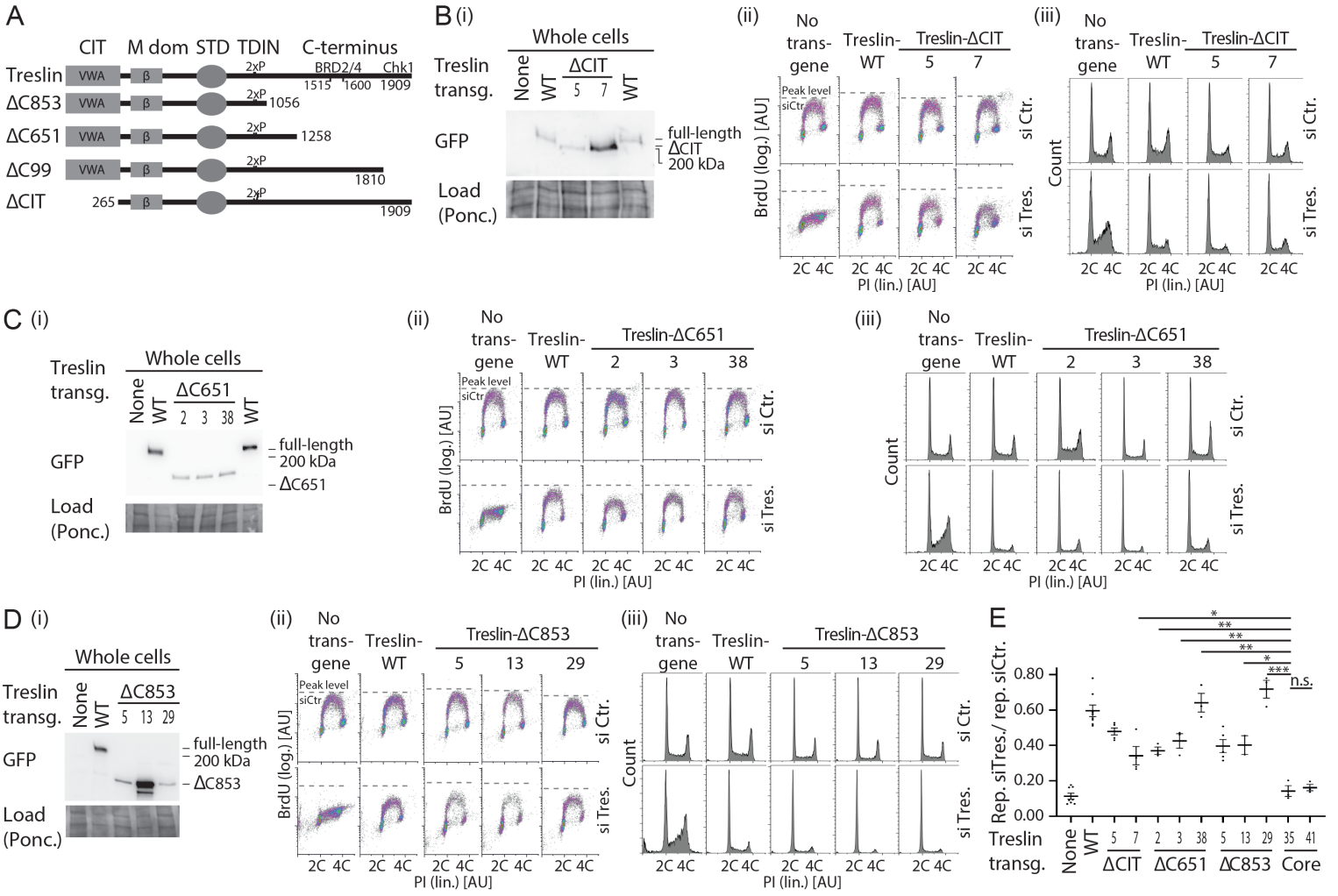
A
CIT
M dom
STD
TDIN
C-terminus
Treslin
ΔC853
ΔC651
ΔC99
ΔCIT
VWA
β
2xP
BRD2/4
Chk1
1515
1600
1909
1056
1258
1810
265
B (i)
Whole cells
Treslin transg.
None
WT
ΔCIT
5
7
GFP
Load (Ponc.)
full-length
ΔCIT
200 kDa
(ii)
No trans-gene
Treslin-WT
Treslin-ΔCIT
Peak level siCtr
BrdU (log.) [AU]
si Ctr.
si Tres.
2C 4C
PI (lin.) [AU]
(iii)
Count
C (i)
ΔC651
2
3
38
full-length
200 kDa
ΔC651
Treslin-ΔC651
D (i)
ΔC853
13
29
full-length
200 kDa
ΔC853
Treslin-ΔC853
E
Rep. siTres./ rep. siCtr.
0.80
0.60
0.40
0.20
0.00
n.s.
Treslin transg.
None
WT
ΔCIT
ΔC651
ΔC853
Core
35
41

Figure S11

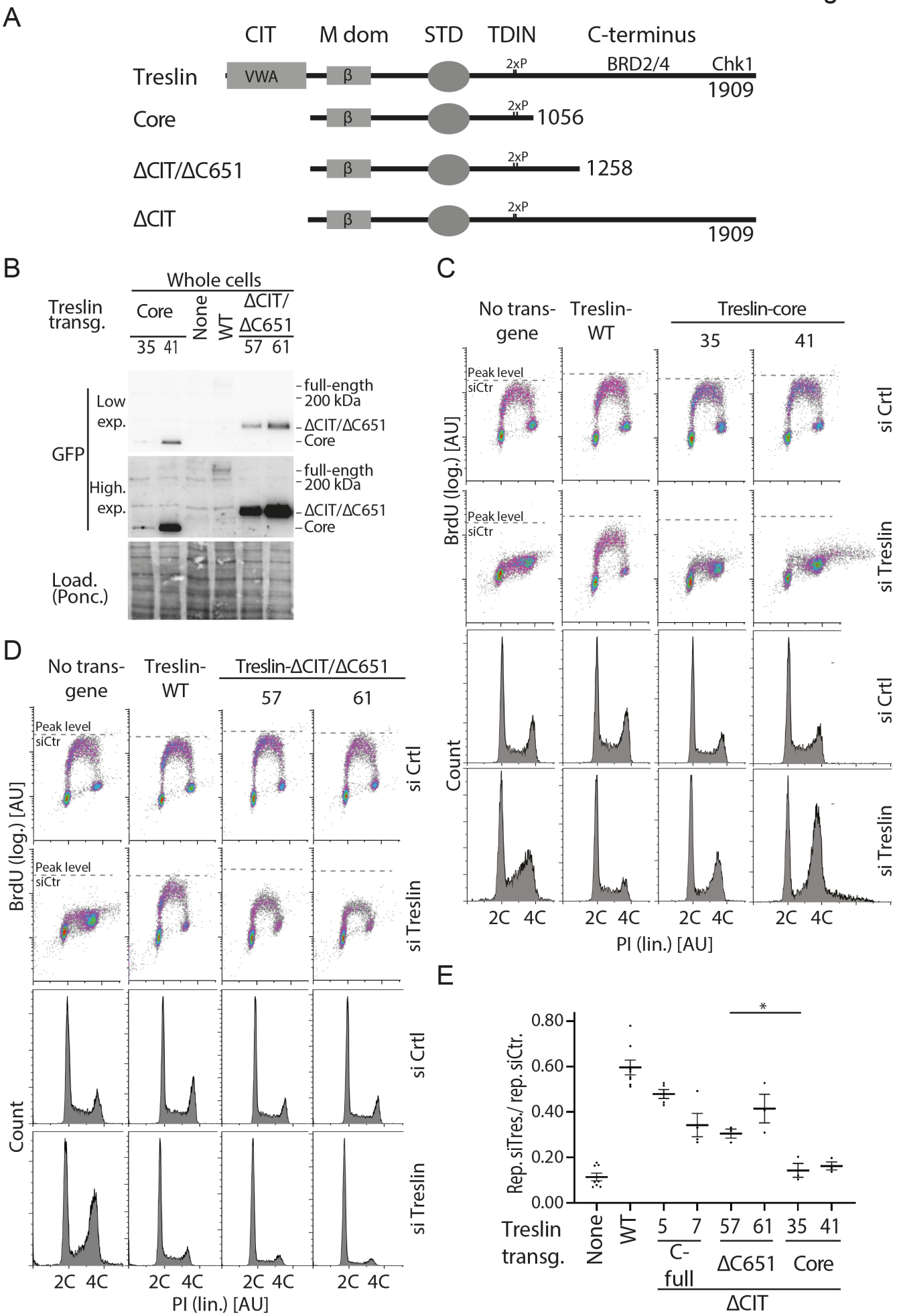
A
CIT
M dom
STD
TDIN
C-terminus
Treslin
VWA
β
2xP
BRD2/4
Chk1
1909
Core
1056
ΔCIT/ΔC651
1258
ΔCIT
B
Whole cells
Treslin transg.
Core
None
WT
ΔCIT/ ΔC651
35 41
57 61
GFP
Low exp.
High. exp.
full-length 200 kDa
ΔCIT/ΔC651
Core
Load. (Ponc.)
C
No trans-gene
Treslin-WT
Treslin-core
35
41
Peak level siCtr
BrdU (log.) [AU]
si Crtl
si Treslin
Count
2C 4C
PI (lin.) [AU]
D
No trans-gene
Treslin-WT
Treslin-ΔCIT/ΔC651
57
61
E
Rep. siTres./ rep. siCtr.
0.80
0.60
0.40
0.20
0.00
*
Treslin transg.
None
WT
5 7
C-full
57 61
ΔC651
35 41
Core
ΔCIT

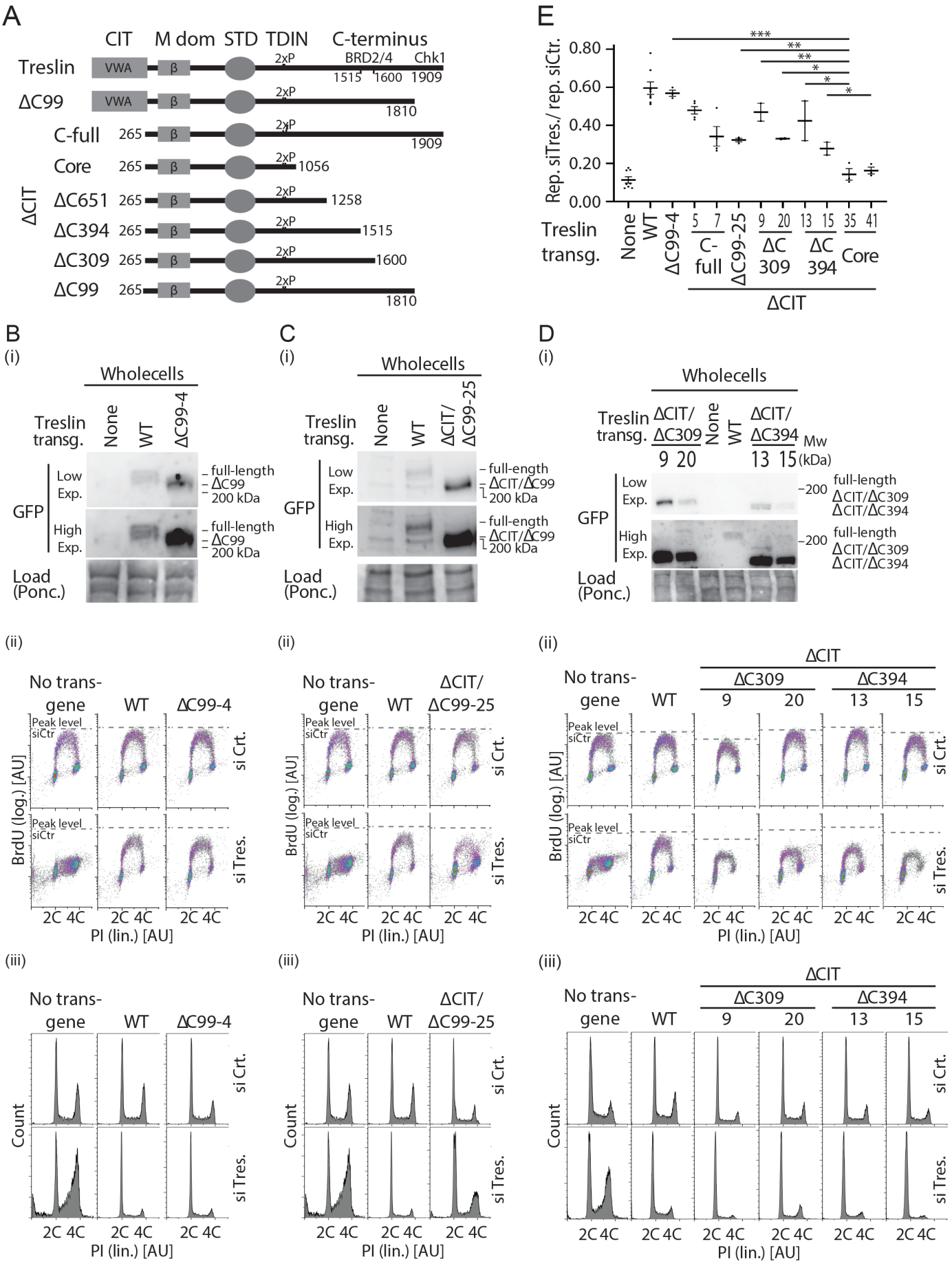
A
CIT
M dom
STD
TDIN
C-terminus
Treslin
VWA
β
2xP
BRD2/4
Chk1
1515
1600
1909
ΔC99
1810
C-full
265
Core
1056
ΔCIT
ΔC651
1258
ΔC394
1515
ΔC309
1600
ΔC99
1810
E
Rep. siTres./ rep. siCtr.
0.80
0.60
0.40
0.20
0.00
***
**
**
*
*
*
Treslin transg.
None
WT
ΔC99-4
5
7
C-full
ΔC99-25
9
20
ΔC 309
13
15
ΔC 394
35
41
Core
ΔCIT
B
(i)
Wholecells
Treslin transg.
None
WT
ΔC99-4
GFP
Low Exp.
High Exp.
full-length
ΔC99
200 kDa
Load (Ponc.)
C
(i)
Wholecells
Treslin transg.
None
WT
ΔCIT/ ΔC99-25
GFP
Low Exp.
High Exp.
full-length
ΔCIT/ΔC99
200 kDa
Load (Ponc.)
D
(i)
Wholecells
Treslin transg.
ΔCIT/ ΔC309
9 20
None
WT
ΔCIT/ ΔC394
13 15
Mw (kDa)
GFP
Low Exp.
High Exp.
200
full-length
ΔCIT/ΔC309
ΔCIT/ΔC394
Load (Ponc.)
(ii)
No trans-gene
WT
ΔC99-4
Peak level siCtr
si Crt.
si Tres.
BrdU (log.) [AU]
2C 4C
PI (lin.) [AU]
(ii)
No trans-gene
WT
ΔCIT/ ΔC99-25
Peak level siCtr
si Crt.
si Tres.
BrdU (log.) [AU]
2C 4C
PI (lin.) [AU]
(ii)
ΔCIT
No trans-gene
WT
ΔC309
9
20
ΔC394
13
15
Peak level siCtr
si Crt.
si Tres.
BrdU (log.) [AU]
2C 4C
PI (lin.) [AU]
(iii)
No trans-gene
WT
ΔC99-4
si Crt.
si Tres.
Count
2C 4C
PI (lin.) [AU]
(iii)
No trans-gene
WT
ΔCIT/ ΔC99-25
si Crt.
si Tres.
Count
2C 4C
PI (lin.) [AU]
(iii)
ΔCIT
No trans-gene
WT
ΔC309
9
20
ΔC394
13
15
si Crt.
si Tres.
Count
2C 4C
PI (lin.) [AU]

Figure S13

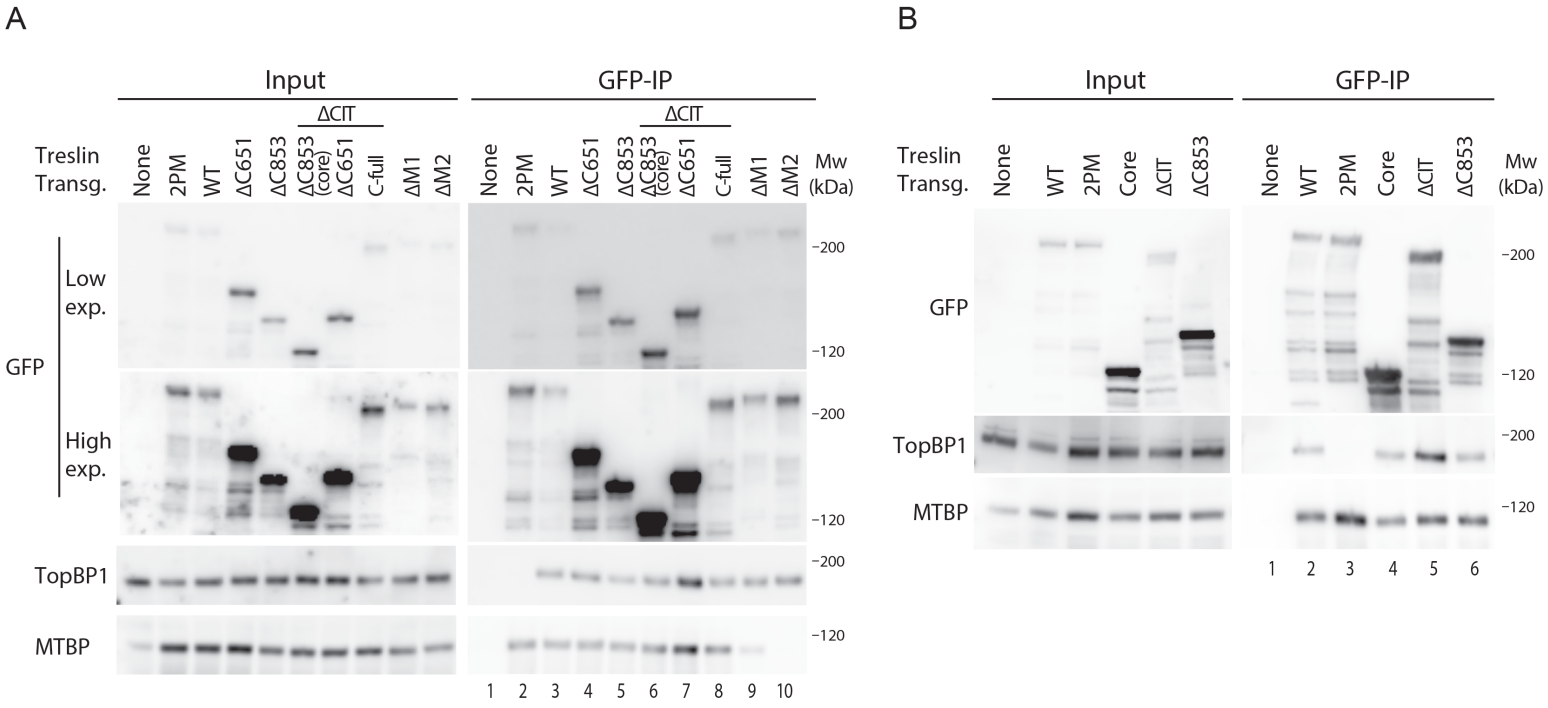
A
Input
GFP-IP
ΔCIT
Treslin Transg.
None
2PM
WT
ΔC651
ΔC853
ΔC853 (core)
ΔC651
C-full
ΔM1
ΔM2
Mw (kDa)
GFP
Low exp.
High exp.
TopBP1
MTBP
200
120
1 2 3 4 5 6 7 8 9 10
B
Input
GFP-IP
Treslin Transg.
None
WT
2PM
Core
ΔCIT
ΔC853
Mw (kDa)
GFP
TopBP1
MTBP
200
120
1 2 3 4 5 6